DEVELOPMENTAL DYNAMICS 246:162–185, 2017
DOI: 10.1002/DVDY.24481

RESEARCH ARTICLE

Hypoxia and Hyperoxia Differentially Control Proliferation of Rat Neural Crest Stem Cells via Distinct Regulatory Pathways of the HIF1α–CXCR4 and TP53–TPM1 Proteins

Chien-Cheng Chen,[1] Ching-Wu Hsia,[2] Cheng-Wen Ho,[1,3] Chang-Min Liang,[4] Chieh-Min Chen,[5] Kun-Lun Huang,[1,6] Bor-Hwang Kang,[7,8] and Yi-Hui Chen[1]*

[1]Graduate Institute of Aerospace and Undersea Medicine, National Defense Medical Center, Neihu District, Taipei City, Taiwan
[2]Department of Finance, School of Management, Shih Hsin University, Wenshan District, Taipei City, Taiwan
[3]Division of Rehabilitation Medicine, Taoyuan Armed Forces General Hospital, Longtan District, Taoyuan City, Taiwan
[4]Department of Ophthalmology, Tri-Service General Hospital, Neihu District, Taipei City, Taiwan
[5]Graduate Institute of Microbiology and Immunology, National Defense Medical Center, Neihu District, Taipei City, Taiwan
[6]Department of Undersea and Hyperbaric Medicine, Tri-Service General Hospital, Neihu District, Taipei City, Taiwan
[7]Division of Diving Medicine, Zuoying Branch of Kaohsiung Armed Forces General Hospital, Zuoying District, Kaohsiung City, Taiwan
[8]Department of Otorhinolaryngology – Head and Neck Surgery, Tri-Service General Hospital, Taipei City, Taiwan

Background: Neural crest stem cells (NCSCs) are a population of adult multipotent stem cells. We are interested in studying whether oxygen tensions affect the capability of NCSCs to self-renew and repair damaged tissues. NCSCs extracted from the hair follicle bulge region of the rat whisker pad were cultured in vitro under different oxygen tensions. Results: We found significantly increased and decreased rates of cell proliferation in rat NCSCs (rNCSCs) cultured, respectively, at 0.5% and 80% oxygen levels. At 0.5% oxygen, the expression of both hypoxia-inducible factor (HIF) 1α and CXCR4 was greatly enhanced in the rNCSC nuclei and was suppressed by incubation with the CXCR4-specific antagonist AMD3100. In addition, the rate of cell apoptosis in the rNCSCs cultured at 80% oxygen was dramatically increased, associated with increased nuclear expression of TP53, decreased cytoplasmic expression of TPM1 (tropomyosin-1), and increased nuclear-to-cytoplasmic translocation of S100A2. Incubation of rNCSCs with the antioxidant *N*-acetylcysteine (NAC) overcame the inhibitory effect of 80% oxygen on proliferation and survival of rNCSCs. Conclusions: Our results show for the first time that extreme oxygen tensions directly control NCSC proliferation differentially via distinct regulatory pathways of proteins, with hypoxia via the HIF1α–CXCR4 pathway and hyperoxia via the TP53–TPM1 pathway. *Developmental Dynamics 246:162–185, 2017*. © 2016 Wiley Periodicals, Inc.

Key words: antioxidant; CDKN1A ($p21^{CIP1/WAF1}$); CXCR4; HIF1α; hyperoxia; hypoxia; neural crest; oxygen; S100A2; stem cells; TP53; TPM1 (tropomyosin-1)

Submitted 20 June 2016; First Decision 9 December 2016; Accepted 13 December 2016; Published online 21 December 2016

Introduction

Oxygen tensions have been demonstrated to play a critical role in regulating stem cell behaviors, including quiescence, self-renewal, proliferation, differentiation, migration, senescence, and apoptosis (Kaindl et al., 2006; Zhu et al., 2006; Lu and Finkel, 2008; Forristal et al., 2010; Mohyeldin et al., 2010; Abdollahi et al., 2011; Raheja et al., 2011; Vieira et al., 2011; Hung et al., 2012; Bigarella et al., 2014; Hakim et al., 2014; Ludin et al., 2014; Shi et al., 2014; Zhou et al., 2014). The neural crest has been called the fourth germ layer and the NCSCs are multipotent stem cells that are capable of differentiating into ectodermal (e.g., neural and glial), mesodermal (mesenchymal), and endodermal (parafollicular) cell types during embryonic development (Manley and Capecchi, 1998; Mansouri et al., 1998; Adams and Bronner-Fraser, 2009; d'Aquino et al., 2011; Baek et al., 2013; Dai et al., 2013a; Shtukmaster et al., 2013; Isern et al., 2014; Jacob et al., 2014; Konig et al., 2014; Kunisada et al., 2014; La Noce et al., 2014; Mishina and Snider, 2014; Schwarz et al., 2014; Shyamala et al., 2015). In adults, NCSCs mainly reside in the enteric nervous system, dorsal root ganglia, bone marrow, cornea, heart, carotid body, skin hair follicle, dental pulp and periodontal ligament, etc. (Gronthos et al., 2002; Kruger et al., 2002; Sieber-Blum et al., 2004; Tomita et al., 2005; Yoshida et al., 2006; Li et al., 2007; Pardal et al., 2007; Yang et al., 2007; Coura et al., 2008; El-Helou et al., 2008; Nagoshi et al., 2008; Sieber-Blum and Hu, 2008;

Grant sponsor: Medical Affairs Bureau–Ministry of National Defense, R.O.C.; Grant numbers: #MAB101-62, MAB105-056.
*Correspondence to: Yi-Hui Chen, Room #8261, Graduate Institute of Aerospace and Undersea Medicine, National Defense Medical Center, Neihu, Taipei 11490, Taiwan. E-mail: yihuichen@mail.ndmctsgh.edu.tw

Article is online at: http://onlinelibrary.wiley.com/doi/10.1002/dvdy.24481/abstract

Stevens et al., 2008; Liu et al., 2009; Clewes et al., 2011; Isern et al., 2014; Mayo et al., 2014).

Previous in vivo studies have shown that hypoxia (10% O_2) increased proliferation and differentiation of mouse and rat NCSCs in the carotid body indirectly and non–cell-autonomously via synaptic-like contacts with the peripheral glomus cells (Kokovay and Temple, 2007; Pardal et al., 2007; Platero-Luengo et al., 2014; Lopez-Barneo et al., 2016a,b). Furthermore, a recent in vivo study published this year demonstrated that hypoxia greatly increased the number of NCSCs in chick embryos via HIF1α-mediated epithelial-to-mesenchymal transition (EMT) (Scully et al., 2016). In addition to in vivo studies, previous in vitro studies have also reported increased colony-forming capacity and multilineage differentiation of NCSCs under hypoxia at 3–6% oxygen levels (Morrison et al., 1999, 2000). On the other hand, an in vivo study of hyperoxia (40% O_2) has reported reduced death and retarded migration of rat NCSCs in the lateral edges of the closing cranial neural folds (CNF) in rat embryos with 10–12 somites, leading to a large kite-shaped, broader than normal CNF (Morriss and New, 1979).

Hypoxia is both a common physiological condition observed in the niches of most types of adult stem cells and a pathological situation occurred in damaged tissues in various types of diseases or traumatic injury (Michiels, 2004; Hu et al., 2009; Hellewell et al., 2010; Mohyeldin et al., 2010). Therefore, hypoxia may play an important role in regulating the self-renewal and regenerative capability of adult stem cells during the process of tissue repair and wound healing. It has been demonstrated that low oxygen tensions (hypoxia) ranging from $\leq$0.5% to 8% O_2 are able to maintain the undifferentiated state and regulate proliferation and cell fate commitment of embryonic, hematopoietic, mesenchymal, and neural stem cells (Mohyeldin et al., 2010). While most previous studies demonstrated that hypoxia promoted proliferation of both embryonic and adult stem cells (Grayson et al., 2007; Lee et al., 2008a; Forristal et al., 2010; Santilli et al., 2010; Hung et al., 2012; Kakudo et al., 2015), there were only a couple studies showing inhibition of embryonic and mesenchymal stem cell proliferation under hypoxia (Fernandes et al., 2010; Holzwarth et al., 2010).

On the other hand, hyperoxia-induced oxidative stress and oxygen toxicity are major issues of concern in the process of ventilatory oxygen therapy or diving (Thorsen et al., 2001; Alcaraz-Garcia et al., 2008; Bitterman, 2010; Martin and Grocott, 2013). Previous studies have demonstrated that an FiO_2 at higher than 90% is lethal and inhibits proliferation and induces apoptosis of both endothelial and epithelial cells via TGFβ-, NF-κB-, or TP53-dependent signaling pathways (Horowitz, 1999; O'Reilly, 2001). In contrast, an FiO_2 at lower than 90% is sublethal and generally stimulates rather than inhibits cell proliferation, and induces apoptosis of endothelial but not epithelial cells (O'Reilly, 2001). In addition, hyperoxia-induced accumulation of reactive oxygen species (ROS) has been reported to promote differentiation, senescence, and apoptosis of multiple stem cell populations (Csete et al., 2001; Bigarella et al., 2014; Ludin et al., 2014; Atashi et al., 2015), suggesting that hyperoxia also plays an important role in regulating the regenerative capability of adult stem cells.

Because there was no previous study reporting the molecular effects of sublethal levels of hyperoxia on NCSC survival and proliferation, and it was not known whether hypoxia could regulate NCSC proliferation cell-autonomously, we were interested in further unraveling the molecular effects of hyperoxia and hypoxia on the cell viability and proliferation of NCSCs. In this study, we extracted NCSCs from the hair follicle bulges of rat whisker pads and cultured rNCSCs at 0.5%, 20%, 40%, and 80% oxygen levels, respectively. We then analyzed the expression levels and patterns of NCSC markers FOXD3 (Kos et al., 2001; Thomas and Erickson, 2009; Mundell and Labosky, 2011; Nelms et al., 2011; Wang et al., 2011; Wahlbuhl et al., 2012; Hochgreb-Hagele and Bronner, 2013), NGFR (also known as p75 neurotrophin receptor) (Wong et al., 2006; Lee et al., 2007; d'Aquino et al., 2011; Sigal et al., 2012; Wen et al., 2012; Dai et al., 2013b), SNAIL (LaBonne and Bronner-Fraser, 2000; del Barrio and Nieto, 2002; Aybar et al., 2003; Lee et al., 2007), and SOX10 (Paratore et al., 2001; Kim et al., 2003; Kelsh, 2006; Wong et al., 2006; Lee et al., 2007; Wahlbuhl et al., 2012), along with markers of proliferation, apoptosis, cell cycle regulation, and cytoskeleton components.

Our results indicated that hypoxia under 0.5% O_2 dramatically increased nuclear expression of HIF1α and CXCR4 as well as decreased CDKN1A ($p21^{CIP1/WAF1}$)-positive nuclei numbers and proliferation rates in rNCSCs without altering apoptosis rates and expression levels and patterns of F-actin, cortactin (CTTN), and TPM1. The enhancing effect of hypoxia on rNCSC proliferation was inhibited by incubation of rNCSCs with the CXCR4-specific antagonist AMD3100 or by transfection of rNCSCs with *Hif1α* siRNA or *Cxcr4*. We also found that hyperoxia under 80% O_2 promoted cytoplasmic translocation of the calcium-binding protein S100A2, inhibited TPM1 expression and proliferation, as well as significantly increased both $TP53^+$ and $CDKN1A^+$ nuclei numbers and apoptosis rates in rNCSCs. The, respectively, inhibitory and enhancing effects of hyperoxia on rNCSC proliferation and apoptosis were both inhibited by *N*-acetylcysteine (NAC) treatment or *Tp53* siRNA transfection of rNCSCs but not by *S100a2* siRNA transfection of rNCSCs. Taken together, our findings demonstrate that 0.5% and 80% oxygen levels differentially control NCSC proliferation via distinct regulatory pathways of the HIF1α–CXCR4 and TP53–TPM1 proteins, respectively.

Results

Analyses of Dissolved Oxygen Concentrations and Neural Crest Marker Expression in the rNCSCs Cultured Under Various Oxygen Tensions

Before culturing under various oxygen tensions, the dissolved oxygen concentration in the rNCSC culture medium was 18.6 ± 0.5% in all culture plates. During the first 12 hr of culturing under hypoxia or hyperoxia, the dissolved oxygen concentration gradually decreased to 1.8 ± 0.3% in the incubator set up at 0.5% O_2 and to 2.4 ± 0.4% in the incubator set up at 1% O_2, and gradually increased to 35.8 ± 0.7% in the incubator set up at 40% O_2 and to 64.5 ± 0.8% in the incubator set up at 80% O_2. Between 18 and 36 hr of culturing, the dissolved oxygen concentration became constant and was 0.3 ± 0.1% in the incubator set up at 0.5% O_2 and 0.8 ± 0.2% in the incubator set up at 1% O_2, and was 39.3 ± 0.3% in the incubator set up at 40% O_2 and 78.9 ± 0.5% in the incubator set up at 80% O_2.

After culturing rNCSCs under various oxygen tensions for 36 hr, we analyzed expression of the neural crest markers NGFR (p75) and the transcription factors FOXD3, SNAIL, and SOX10 in rNCSCs. The expression levels and patterns of

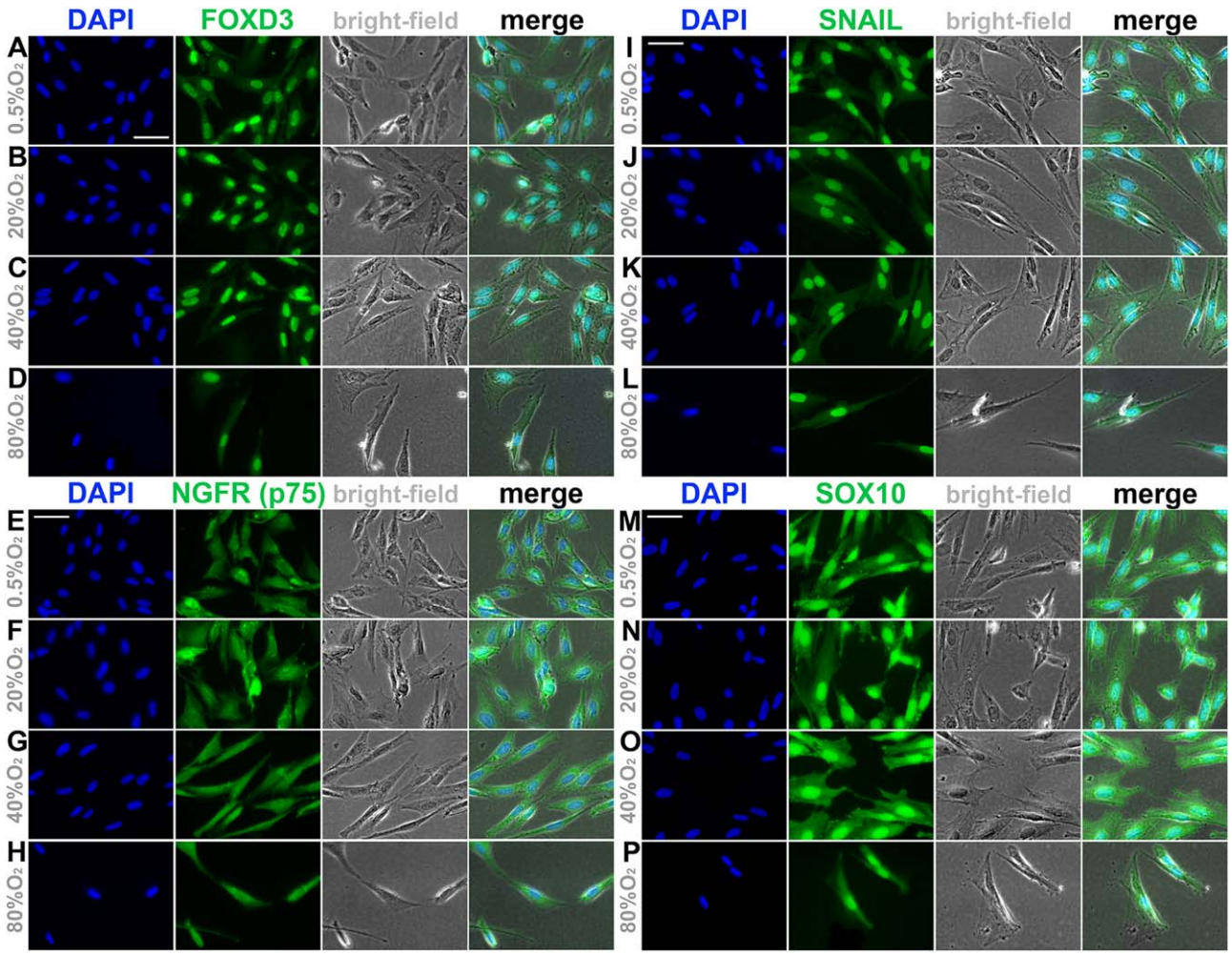

Fig. 1. **A–P**: Normal expression of neural crest markers in rNCSCs cultured under various oxygen tensions. Immunostaining against neural crest markers NGFR, FOXD3, SNAIL and SOX10 (green) revealed that the nuclei of all rNCSCs cultured at 0.5% (A, E, I, and M), 20% (B, F, J, and N), 40% (C, G, K, and O), and 80% (D, H, L, and P) oxygen tensions for 36 hr expressed all of the three neural crest markers. In all rNCSCs cultured under various oxygen tensions, NGFR was predominantly expressed in the cytoplasm (A–D), and FOXD3, SNAIL and SOX10 were all predominantly expressed in the nuclei (E–H, I–L, and M–P), in agreement with the previously reported expression patterns of these markers (Sieber-Blum et al., 2004; Wong et al., 2006; Lee et al., 2007; Thomas and Erickson, 2009; Mundell and Labosky, 2011; Wen et al., 2012; Kerosuo et al., 2015). The scale bars in panels A, E, I, and M apply to panels A–D, E–H, I–L, and M–P, respectively. All four scale bars in panels A, E, I, and M = 50 μm.

FOXD3, NGFR, SNAIL and SOX10 were all comparable among rNCSCs cultured at 0.5%, 20%, 40%, and 80% O_2 (compare the panels A–D, E–H, I–L, and M–P in Fig. 1). NGFR showed predominantly cytoplasmic expression in all rNCSCs, and also showed strong nuclear expression in 34.2 ± 1.4% of the rNCSCs cultured at 0.5% O_2, in 37.5 ± 1.8% of the rNCSCs cultured at 20% O_2, in 36.3 ± 2.2% of the rNCSCs cultured at 40% O_2, and in 31.8 ± 1.5% of the rNCSCs cultured at 80% O_2 ($n = 12$; $P > 0.05$, one-way analysis of variance [ANOVA]) (Fig. 1E–H). On the other hand, FOXD3, SNAIL, and SOX10 all displayed predominantly nuclear expression (Fig. 1A–D, I–L, and M–P). The expression patterns of FOXD3, NGFR, SNAIL, and SOX10 in rNCSCs cultured under various oxygen tensions were all in agreement with previous studies (Sieber-Blum et al., 2004; Wong et al., 2006; Lee et al., 2007; Thomas and Erickson, 2009; Mundell and Labosky, 2011; Wen et al., 2012; Kerosuo et al., 2015). Our results indicate that neither hypoxia nor hyperoxia affects expression of the neural crest markers FOXD3, NGFR, SNAIL and SOX10 in rNCSCs.

Significant Changes in the Total Cell Numbers and Viability of the rNCSCs Cultured Under Hypoxia or Hyperoxia

Interestingly, we found that 0.5% and 80% oxygen tensions, respectively, increased and decreased the total cell numbers and viability of rNCSCs significantly, and the effects persisted for at least 36 hr after culturing (Fig. 2). While the doubling time of the rNCSCs cultured at 20% and 40% O_2 was 20.74 ± 4.12 hr, the doubling time of the rNCSCs cultured at 0.5% O_2 was only 14.46 ± 2.25 hr ($n = 12$, $P < 0.05$, one-way ANOVA), indicating significantly increased division rates of rNCSCs under hypoxia. On the other hand, for the rNCSCs cultured at 80% O_2, the total cell number kept decreasing rather than increasing between 12 and 36 hr of culturing ($n = 12$, $P < 0.05$ after 12 hr, $P < 0.01$ after 24 and 36 hr, one-way ANOVA), and was decreased to averagely only 37% of the starting cell number (which was 6×10^4 cells/ml) after 36 hr of culturing (Fig. 2A).

The dramatically reduced total number of the rNCSCs cultured at 80% O_2 may result from high rates of cell death under hyperoxia. In

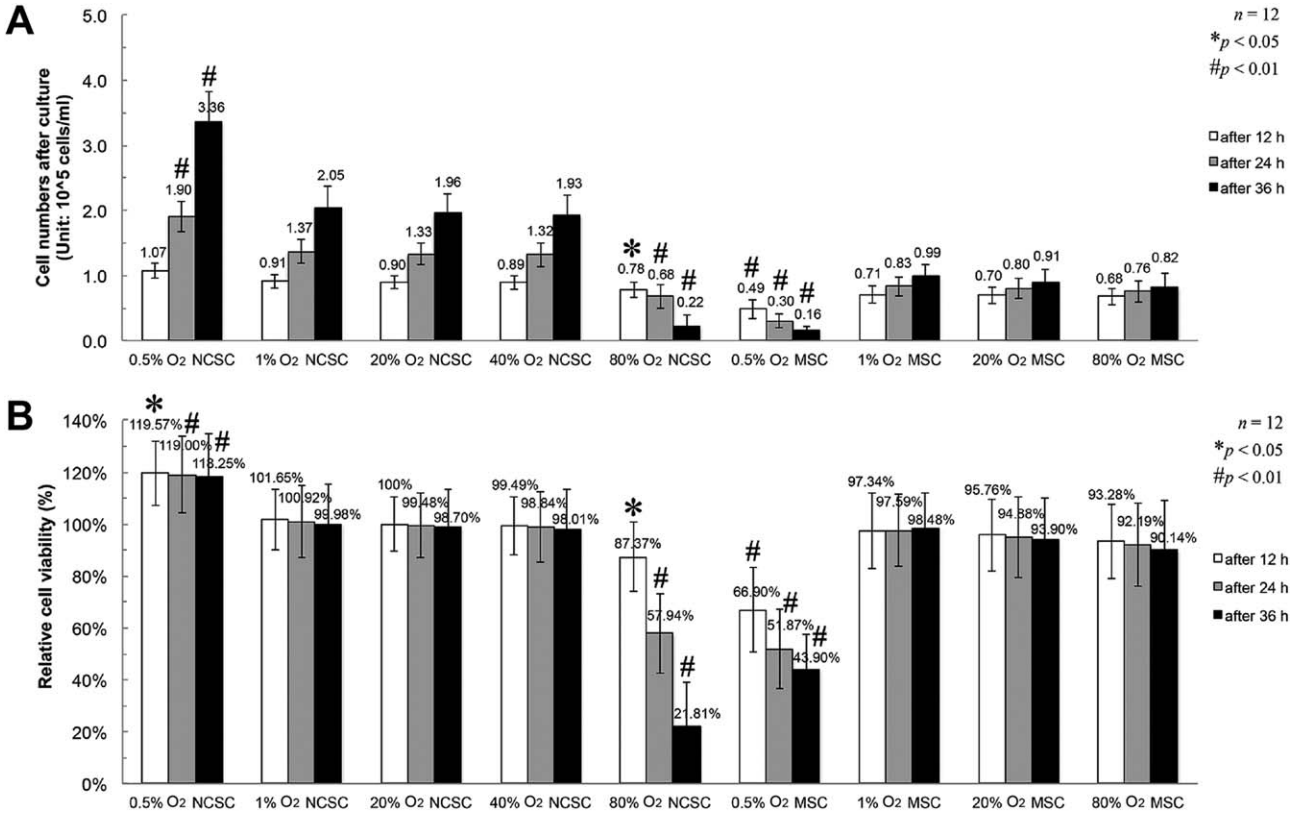

Fig. 2. **A,B**: Significantly increased and decreased total cell numbers and viability of the rNCSCs cultured, respectively, at 0.5% and 80% O_2 for 12, 24, and 36 hr. A: rNCSCs and rMSCs were separately cultured at the same density of 6×10^4 (i.e., 0.6×10^5) cells/ml under various oxygen tensions, and the total cell numbers in units of 10^5 cells/ml after 12, 24, and 36 hr of culturing are shown in the statistical histogram. It is noteworthy that the rNCSCs cultured at 1%, 20%, and 40% O_2 showed comparable total cell numbers at all time points, whereas the rNCSCs cultured at 0.5% O_2 showed significantly increased total cell numbers after 24 and 36 hr compared with the other groups of rNCSCs ($n = 12$, $P < 0.01$, one-way ANOVA). On the other hand, the rNCSCs cultured at 80% O_2 displayed the lowest total cell numbers at all time points among all groups of rNCSCs ($n = 12$, $P < 0.05$ after 12 hr, $P < 0.01$ after 24 and 36 hr, one-way ANOVA). The rMSCs cultured at 0.5% O_2 showed the lowest total cell numbers at all time points among all groups of rMSCs ($n = 12$, $P < 0.01$, one-way ANOVA), whereas there was no statistically significant difference in total cell numbers among the rMSCs cultured at 1%, 20%, and 80% O_2 at all time points ($n = 12$, $P > 0.05$, one-way ANOVA). B: In agreement with the changes in total cell numbers, the highest cell viabilities ($119.57 \pm 12.37\%$, $119.00 \pm 14.64\%$, and $118.25 \pm 16.38\%$) after 12, 24, and 36 hr of culturing were observed in the rNCSCs cultured at 0.5% O_2 ($n = 12$, $P < 0.05$ after 12 hr, $P < 0.01$ after 24 and 36 hr, one-way ANOVA), whereas the lowest cell viabilities among all groups of rNCSCs and rMSCs at each time point were detected, respectively, in the rNCSCs cultured at 80% O_2 ($87.37 \pm 13.24\%$ after 12 hr, $57.94 \pm 15.38\%$ after 24 hr, and $21.81 \pm 17.25\%$ after 36 hr) ($n = 12$, $P < 0.05$ after 12 hr, $P < 0.01$ after 24 and 36 hr, one-way ANOVA) and in the rMSCs cultured at 0.5% O_2 ($66.90 \pm 16.33\%$ after 12 hr, $51.87 \pm 15.29\%$ after 24 hr, and $43.90 \pm 13.87\%$ after 36 hr) ($n = 12$, $P < 0.01$, one-way ANOVA). The viability of the rNCSCs cultured at 20% O_2 after 12 hr was set up as the control value (i.e., 100% viability). The asterisks (*) indicate $P < 0.05$, and the hashtags (#) indicate $P < 0.01$.

consistency with the significantly decreased total numbers of rNCSCs under hyperoxia, the viability of the rNCSCs cultured at 80% O_2 also dramatically decreased from $87.37 \pm 13.24\%$ after 12 hr of culturing to $21.81 \pm 17.25\%$ after 36 hr of culturing ($n = 12$, $P < 0.05$ after 12 hr, $P < 0.01$ after 24 and 36 hr, one-way ANOVA), with a totally 25% decrease of viability (Fig. 2B). In contrast, the average viability of the rNCSCs cultured at 0.5%, 1%, 20%, or 40% O_2 displayed a less than 3% variation between 12 and 36 hr of culturing ($n = 12$, $P > 0.05$, one-way ANOVA) (Fig. 2B). It is noteworthy that the total cell numbers and viability of the rNCSCs cultured at 1% O_2 and 40% O_2 were comparable to the total number and viability of the rNCSCs cultured at 20% O_2 (Fig. 2A,B).

To elucidate whether the, respectively, enhancing and inhibitory effects of 0.5% O_2 and 80% O_2 on cell viability was specific to rNCSCs or a general trend to any type of cells, we also analyzed the total cell numbers and viability of rat bone marrow mesenchymal stem cells (rMSCs) under various oxygen tensions. Of interest, the rMSCs cultured at 0.5% O_2 showed significantly and gradually decreased total numbers and viability after 12, 24, and 36 hr of culturing ($n = 12$, $P < 0.01$, one-way ANOVA), whereas the rMSCs cultured at 1%, 20%, and 80% O_2 displayed no significant difference in total cell numbers and viability after culturing for 12, 24, and 36 hr ($n = 12$, $P > 0.05$, one-way ANOVA) (Fig. 2A,B). Therefore, 0.5% O_2 exerts an enhancing effect on the viability and division rate of rNCSCs and an inhibitory effect on the viability of rMSCs, while 80% O_2 exerts an inhibitory effect on the viability of rNCSCs but not that of rMSCs. Hence the, respectively, enhancing and inhibitory effects of 0.5% and 80% O_2 on cell viability are rNCSC-specific.

Significantly Increased and Decreased Total Numbers and Proliferation of rNCSCs in the Whisker Hair Follicle Tissues Respectively Exposed to Hypoxia and Hyperoxia In Vivo

We were interested in analyzing whether the, respectively, enhancing and inhibitory effects of 0.5% and 80% O_2 on the total

numbers and viability of rNCSCs in vitro recapitulate the effects of hypoxia and hyperoxia on the numbers and proliferation/survival of rNCSCs in the hair follicles in vivo. While the rat whisker hair follicle tissues that had been exposed to normoxia ($21.0 \pm 0.5\%$ O_2) for 36 hr showed no positive signal for hypoxyprobe-1 immunostaining (Fig. 3A) and barely detectable CellROX® Green-positive staining signals (Fig. 3B), the hair follicles exposed to hypoxia ($7.0 \pm 0.5\%$ O_2) and hyperoxia ($89.0 \pm 0.5\%$ O_2) for 36 hr, respectively, displayed extensive staining signals of hypoxyprobe-1 (green in Fig. 3A) and CellROX® Green (green in Fig. 3B) spanning the sebaceous glands, bulge region, and dermal papilla. The increases of the percentages of hypoxyprobe-1^+ and CellROX® $Green^+$ nuclei under hypoxia and hyperoxia, respectively, were both statistically significant ($n = 6$, $P < 0.05$, Mann-Whitney *U*-test) (Fig. 3D,E).

In addition, in comparison with the whisker hair follicles exposed to normoxia, the hair follicles exposed to hypoxia and hyperoxia displayed, respectively, increased and decreased percentages of $SOX10^+$ and $BrdU^+$ nuclei ($n = 6$, $P < 0.05$, one-way ANOVA) (Fig. 3A–C,F), and the hair follicles exposed to hyperoxia also exhibited significantly increased percentages of $TUNEL^+$ nuclei ($n = 6$, $P < 0.05$, one-way ANOVA) (Fig. 3C,F). The immunostaining results indicated increased proliferation and total numbers of $SOX10^+$ rNCSCs in the whisker hair follicles in association with hypoxia, as well as increased apoptosis and decreased proliferation and total numbers of $SOX10^+$ rNCSCs in the hair follicles in association with hyperoxia.

Significantly Increased Proliferation and Nuclear Expression of HIF1α and CXCR4 in the rNCSCs Cultured at 0.5% O_2 In Vitro

Double immunostaining against EdU and the cyclin-dependent kinase inhibitor CDKN1A ($p21^{CIP1/WAF1}$), which is a well-documented suppressor of cell proliferation (Chew et al., 2011; Lin et al., 2013; Wang et al., 2014), revealed a significantly increased percentage of EdU^+ nuclei and decreased percentage of $CDKN1A^+$ nuclei in the rNCSCs cultured at 0.5% O_2 ($n = 12$, $P < 0.01$, one-way ANOVA) (Fig. 4A,G), and a greatly decreased proliferation rate and increased percentage of $CDKN1A^+$ nuclei in the rNCSCs cultured at 80% O_2 ($n = 12$, $P < 0.01$, one-way ANOVA) (Fig. 4D,G). It is noteworthy that $CDKN1A^+$ nuclei were stained with a low level of EdU (indicated by arrows in Fig. 4) or no EdU at all, consistent with the role of CDKN1A in suppressing cell proliferation (Chew et al., 2011; Lin et al., 2013; Wang et al., 2014).

While the proliferation rate of the rNCSCs cultured at 0.5% O_2 was increased to approximately 1.2-fold of the rates of the rNCSCs at 20% and 40% O_2, the proliferation rate of the rNCSCs cultured at 80% O_2 was decreased to less than 20% of the rates of the rNCSCs at 20% and 40% O_2 (Fig. 4G; $n = 12$, $P < 0.01$, one-way ANOVA). On the other hand, the average percentage of $CDKN1A^+$ nuclei in the rNCSCs cultured at 0.5% O_2 was decreased to approximately 30% of the percentages in the rNCSCs at 20% and 40% O_2, whereas the average percentage of $CDKN1A^+$ nuclei in the rNCSCs cultured at 80% O_2 was increased to more than two-fold of the percentages in the rNCSCs at 20% and 40% O_2 (Fig. 4; $n = 12$, $P < 0.01$, one-way ANOVA).

Previous studies have shown that HIF1α and its downstream effector CXCR4 both up-regulate proliferation of various tumor and progenitor cells (Carmeliet et al., 1998; Goda et al., 2003; Kahn et al., 2004; Nombela-Arrieta et al., 2013; Park et al., 2013; Xia et al., 2014; Guimaraes-Camboa et al., 2015), and also up-regulate chemotaxis, migration, and EMT of neural crest stem/progenitor cells in zebrafish, *Xenopus* and chick embryos as well as mouse hair follicles (Belmadani et al., 2009; Rezzoug et al., 2011; Barriga et al., 2013; Singleton Escofet, 2013; Scully et al., 2016). Hence, we were interested in analyzing HIF1α and CXCR4 expression in rNCSCs under various oxygen tensions. Double immunostaining revealed low intensities of HIF1α and CXCR4 signals in the cytoplasm of the rNCSCs cultured at 20%, 40%, and 80% O_2, with CXCR4 mainly expressed in the perinuclear regions (Fig. 5B–D). Interestingly, both HIF1α and CXCR4 signals showed dramatically increased intensities and colocalization in the nuclei of the rNCSCs cultured at 0.5% O_2 (Fig. 5A). The average percentages of both $HIF1\alpha^+$ and $CXCR4^+$ nuclei in the rNCSCs cultured at 0.5% O_2 were increased to more than 30-fold of the percentages in the rNCSCs at 20%, 40%, and 80% O_2 (Fig. 5E; $n = 12$, $P < 0.01$, one-way ANOVA). In addition, it is noteworthy that plasma membrane expression of CXCR4 was detected only in the rNCSCs cultured at 0.5% O_2 (indicated by arrows in Fig. 5A) but not in the rNCSCs cultured at 20%, 40%, or 80% O_2 (Fig. 5B–D).

To evaluate the association between increased nuclear expression of HIF1α and CXCR4 and increased proliferation of rNCSCs during culturing under hypoxia, we incubated rNCSCs with the CXCR4-specific antagonist AMD3100, which has been reported to induce both the internalization of cell surface CXCR4 and down-regulation of CXCR4 protein expression (Kim et al., 2010; Spinello et al., 2011). Of interest, incubation of rNCSCs with 10 μM AMD3100 in the medium during culturing at 0.5% O_2 for 36 hr significantly decreased nuclear expression of CXCR4 without affecting nuclear expression of HIF1α (Fig. 5E,F). We also found that AMD3100 treatment significantly increased the total cell numbers and percentage of $CDKN1A^+$ nuclei as well as decreased the cell viability and percentage of EdU^+ nuclei in the rNCSCs cultured at 0.5% O_2 to the levels comparable to those in the rNCSCs cultured at 20% O_2 (Figs. 4G, 5G,H). It is also noteworthy that the cytoplasmic expression level of CXCR4 in the AMD3100-treated rNCSCs cultured at 0.5% O_2 (indicated by arrows in Fig. 5F) was higher than the levels in the rNCSCs cultured at 20%, 40%, or 80% O_2 (compare Fig. 5F with Fig. 5B–D).

Similar to the effects of AMD3100 treatment, transfection of the rNCSCs cultured at 0.5% O_2 with either *Cxcr4* or *Hif1α* siRNA also significantly decreased the total cell numbers and viability after 12, 24, and 36 hr as well as nuclear expression of CXCR4 to the levels comparable to those in the rNCSCs cultured at 20% O_2 (Figs. 5G,H, 6). Western blot analyses revealed dramatically reduced CXCR4 expression in the nuclei of the rNCSCs cultured at 0.5% O_2 after incubation with AMD3100 or transfection with *Hif1α* or *Cxcr4* siRNA (Fig. 6). In rNCSC nuclei, the protein levels of CXCR4 and HIF1α at 0.5% O_2 were, respectively, more than 11- and 6-fold of the levels at 20%, 40%, and 80% O_2 (Fig. 6; $n = 12$, $P < 0.01$, one-way ANOVA). In the rNCSCs cultured at 0.5% O_2, AMD3100 treatment and *Hif1α* siRNA transfection, respectively, decreased the nuclear expression levels of CXCR4 to averagely 1.38- and 1.15-fold of the level in the rNCSCs cultured at 20% O_2 (Fig. 6; $n = 12$, $P > 0.05$ in comparison with the expression level at 20% O_2, one-way ANOVA). It is noteworthy that, after *Cxcr4* siRNA transfection, the CXCR4 protein level was significantly decreased to averagely 48% of the level in the

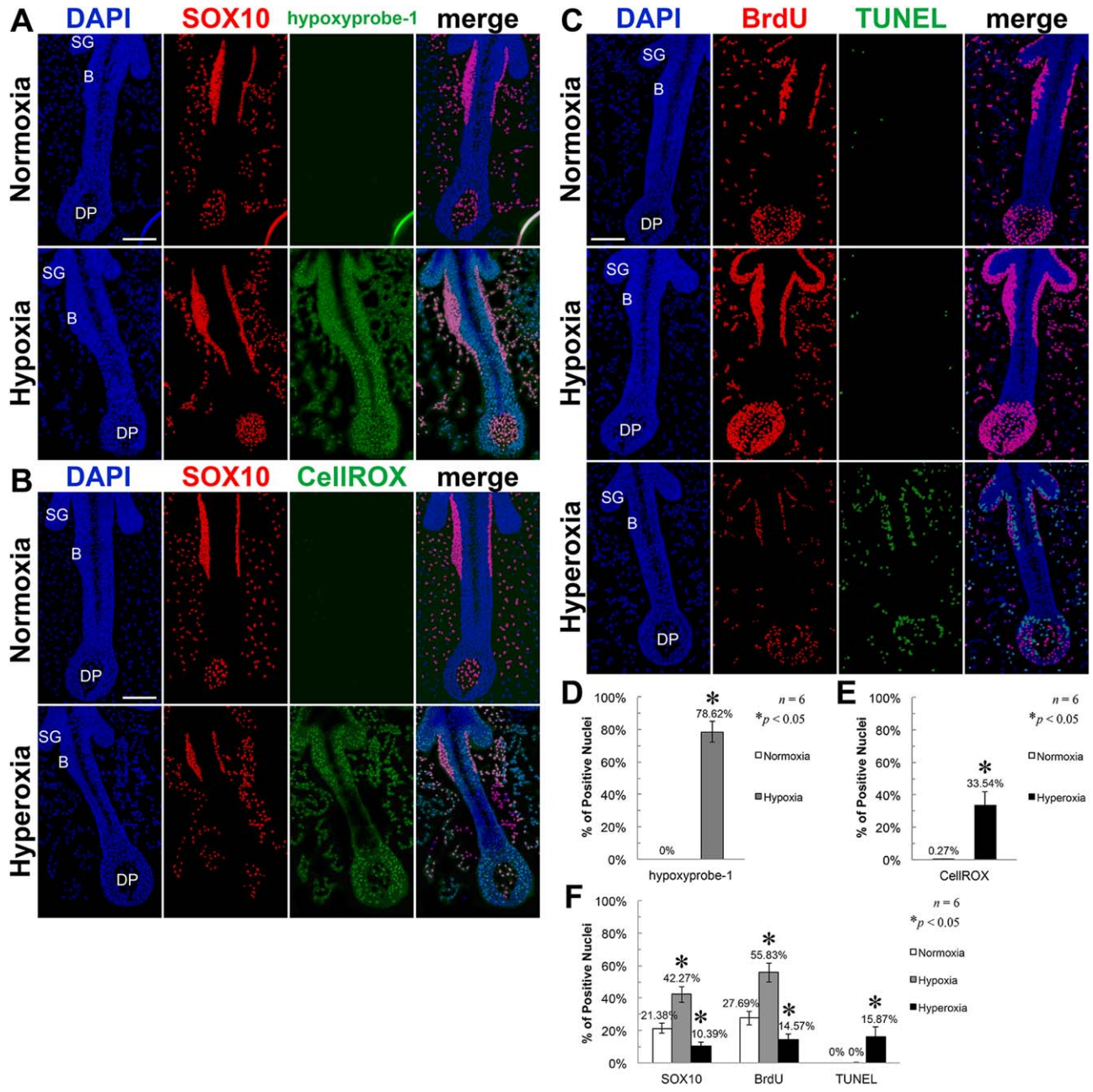

Fig. 3. **A–F**: Significantly increased and decreased total numbers and proliferation of rNCSCs in the whisker hair follicle tissues of the Sprague-Dawley rats, respectively, exposed to hypoxia and hyperoxia. Immunostaining analyses of the whisker hair follicle tissues of the Sprague-Dawley rats exposed to various oxygen tensions for 36 hr showed extensive staining signals of hypoxyprobe-1 (green in A) under hypoxia (A) and of CellROX® Green (green in B) under hyperoxia (B), which spanned the sebaceous glands, bulge region, and dermal papilla, whereas there was no positive signal of hypoxyprobe-1 staining (A) and barely detectable CellROX® Green$^+$ signals (B) in the whisker hair follicles under normoxia. Immunostaining analyses also revealed significantly increased and decreased percentages of SOX10$^+$ and BrdU$^+$ nuclei in the whisker hair follicles under hypoxia and hyperoxia, respectively, in comparison with the percentages in the hair follicles under normoxia (red signals in A–C). The results indicated significantly increased and decreased total numbers and proliferation of rNCSCs in the whisker hair follicles under hypoxia and hyperoxia, respectively. In addition, the percentages of TUNEL$^+$ nuclei in the whisker hair follicles under hyperoxia were significantly increased compared with the percentages under normoxia (green signals in C), indicating significantly increased cell apoptosis in the hair follicles under hyperoxia. The statistical histograms in D–F summarize the percentages of hypoxyprobe-1$^+$, CellROX® Green$^+$, SOX10$^+$, BrdU$^+$, and TUNEL$^+$ nuclei in the hair follicle regions of the whisker pad tissue sections obtained from the Sprague-Dawley rats exposed to normoxia, hypoxia, and hyperoxia. Mann-Whitney *U*-test with $n = 6$ was applied for hypoxyprobe-1 and CellROX® Green staining, and one-way ANOVA with $n = 6$ was applied for SOX10, BrdU, and TUNEL staining, and the asterisks (*) indicate $P < 0.05$. Abreviations: B, bulge region; DP, dermal papilla; SG, sebaceous gland. The scale bars in A, B and C all = 25 μm.

rNCSCs cultured at 20% O_2 (Fig. 6; $n = 12$, $P < 0.05$, one-way ANOVA). Of interest, neither AMD3100 treatment nor *Cxcr4* siRNA transfection significantly affected the expression levels of HIF1α in the rNCSC nuclei at 0.5% O_2, which were still significantly increased to more than five-fold of the level in the rNCSCs cultured at 20% O_2 (Fig. 6; $n = 12$, $P < 0.01$, one-way ANOVA).

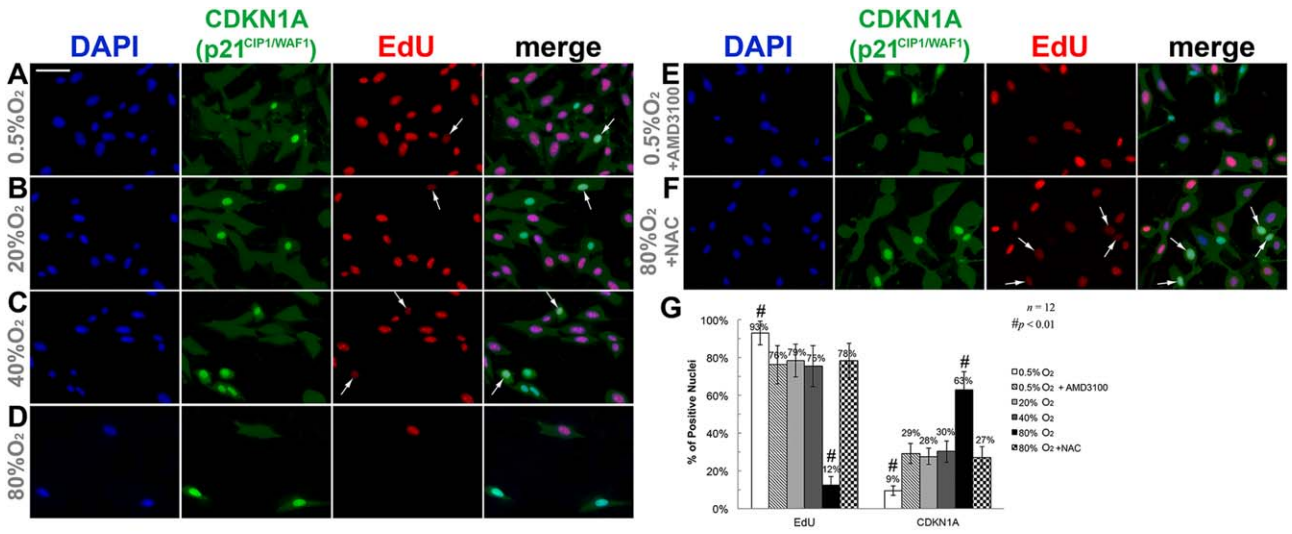

Fig. 4. **A–G**: Significantly decreased and increased percentages of CDKN1A(p21$^{CIP1/WAF1}$)$^+$ nuclei were, respectively, associated with significantly increased and decreased proliferation of the rNCSCs cultured, respectively, at 0.5% and 80% O_2 for 36 hr. Double immunostaining revealed a significantly decreased percentage of CDKN1A$^+$ nuclei (green) and a greatly increased percentage of EdU$^+$ nuclei (red) in the rNCSCs cultured at 0.5% O_2 for 36 hr ($n = 12$, $P < 0.01$, one-way ANOVA) (A,G), as well as a greatly increased percentage of CDKN1A$^+$ nuclei (green) and a dramatically decreased percentage of EdU$^+$ nuclei (red) in the rNCSCs cultured at 80% O_2 for 36 hr ($n = 12$, $P < 0.01$, one-way ANOVA) (E,G), indicating significantly increased and decreased proliferation of the rNCSCs cultured, respectively, under hypoxia and hyperoxia. Incubation with AMD3100 at 0.5% O_2 and with NAC at 80% O_2, respectively, decreased and increased proliferation of the rNCSCs to the levels comparable to that in the rNCSCs cultured at 20% or 40% O_2 ($n = 12$, $P > 0.05$, one-way ANOVA) (compare panels E and F with B and C). CDKN1A$^+$ nuclei were stained with a low level of EdU (indicated by arrows) or no EdU at all. The scale bar in A represents 50 μm and applies to panels A–F. The statistical histogram in (G) summarizes the percentages of EdU$^+$ and CDKN1A$^+$ nuclei in the rNCSCs cultured under various oxygen tensions and with different drug treatments. One-way ANOVA with $n = 12$ was applied, and the hashtags (#) indicate $P < 0.01$.

Significantly Decreased Proliferation and TPM1 Expression and Increased Apoptosis and TP53 Expression as Well as Nuclear-to-Cytoplasmic Translocation of S100A2 in the rNCSCs at 80% O_2 In Vitro

In the rNCSCs cultured at 80% O_2, in addition to the greatly decreased proliferation rate (Fig. 4D,G), we also observed dramatically increased percentages of TP53$^+$ and TUNEL$^+$ nuclei in comparison to the rNCSCs cultured at 0.5%, 20%, and 40% O_2 (compare among panels A–D in Fig. 7, and see also Fig. 7F). Double immunostaining against TUNEL and the tumor suppressor TP53, which is a critical inducer of cell apoptosis (Chipuk et al., 2004; Timofeev et al., 2013), revealed nuclear colocalization of TUNEL$^+$ and TP53$^+$ staining signals (indicated by arrows in Fig. 7), and that the average percentages of both TP53$^+$ and TUNEL$^+$ nuclei in the rNCSCs cultured at 80% O_2 were increased to more than 60-fold of the percentages in the rNCSCs cultured at 20% O_2 (Fig. 7F; $n = 12$, $P < 0.01$, one-way ANOVA).

It has been reported that in keratinocytes, which are colocalized with NCSCs in the epidermal niche in adult hair follicle bulge regions (Sieber-Blum and Grim, 2004; Cichorek et al., 2013), oxidative stress induces nuclear-to-cytoplasmic translocation of the calcium-binding protein S100A2 (Zhang et al., 2002), which has been shown to interact with both TP53 and tropomyosin and modulate their respective activity or conformation (Gimona et al., 1997; Mueller et al., 2005). As dramatically increased nuclear expression of TP53 was observed in the rNCSCs cultured at 80% O_2 (Fig. 7), we were interested in analyzing whether hyperoxia also affected expression and intracellular localization of S100A2 in rNCSCs.

Of interest, similar to the effect of oxidative stress on human keratinocytes, we observed dramatically increased nuclear-to-cytoplasmic translocation of S100A2 in all of the rNCSCs cultured at 80% O_2 (indicated by arrows in Fig. 8D) and in only a few rNCSCs cultured under lower oxygen tensions (Fig. 8B,C). Double immunostaining revealed that the rNCSCs expressing S100A2 in the cytoplasm instead of the nucleus showed strong nuclear expression of TP53 (indicated by arrows in Fig. 8B–D). Consistent with the double immunostaining results, our Western blot analyses indicated that the protein levels of S100A2 and TP53 in the nuclei of the rNCSCs cultured at 80% O_2, respectively, decreased to only 16.6% and increased to more than nine-fold of the levels in the rNCSCs cultured at 20% O_2 ($n = 12$, $P < 0.01$, one-way ANOVA) (Fig. 9A,B).

We found that incubation of the rNCSCs with 1 mM of the antioxidant NAC in the medium during culturing at 80% O_2 for 36 hr was sufficient to inhibit nuclear-to-cytoplasmic translocation of S100A2 and decrease TP53 expression to the levels comparable with those in the rNCSCs cultured at 20% O_2 ($n = 12$, $P > 0.05$, one-way ANOVA) (Figs. 8E,F, 9A,B). Interestingly, overexpression of *Tp53* by transfection of the *CMV*-containing *Tp53* expression vector (*Tp53 CMV*) into the rNCSCs cultured at 20% O_2 did not increase nuclear-to-cytoplasmic translocation of S100A2 (Figs. 8I, 9A,B), and knockdown of *Tp53* by transfection of *Tp53* siRNA into the rNCSCs cultured at 80% O_2 did not inhibit nuclear-to-cytoplasmic translocation of S100A2 (Figs. 8J, 9A,B), either. These results demonstrated that the dramatically increased nuclear-to-cytoplasmic translocation of S100A2 in the rNCSCs

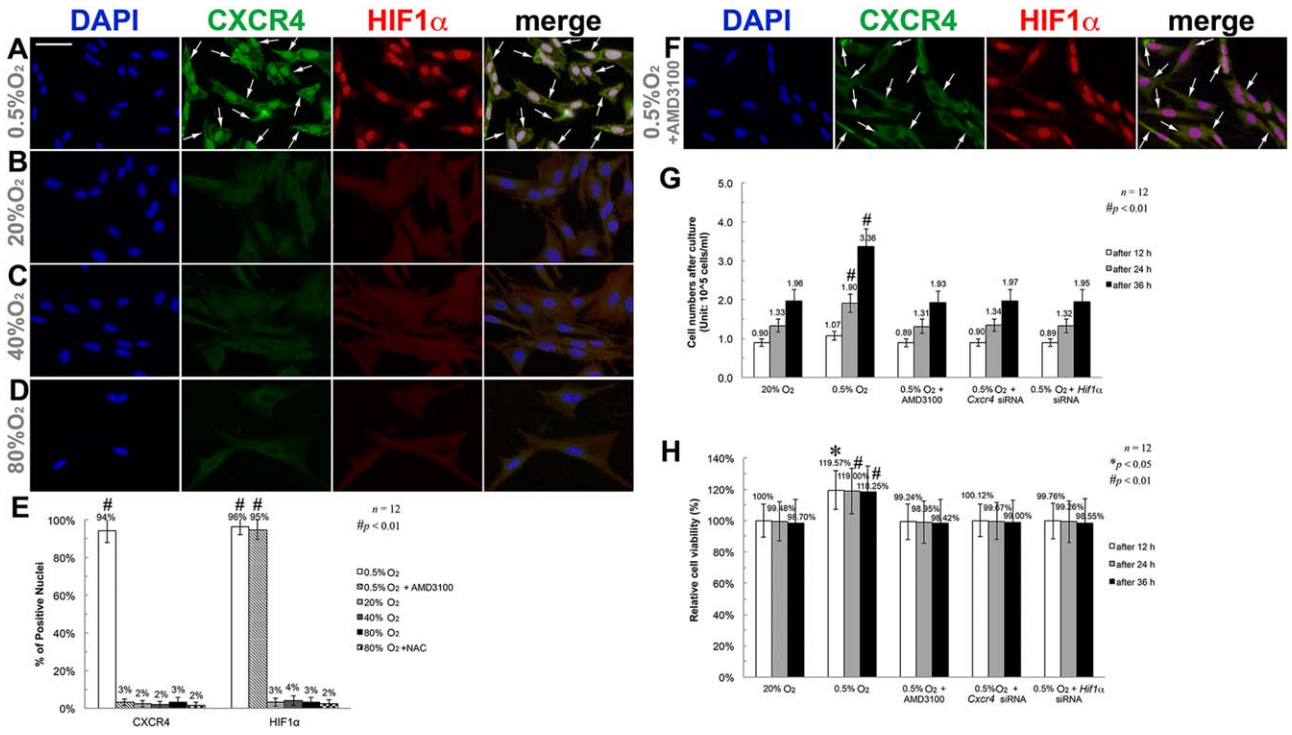

Fig. 5. **A–H**: Dramatically increased nuclear expression of CXCR4 and HIF1α and plasma membrane expression of CXCR4 in the rNCSCs cultured at 0.5% O_2 for 36 hr. Double immunostaining revealed strong expression of both CXCR4 (green) and HIF1α (red) in the nuclei and also apparent expression of CXCR4 on the plasma membrane (indicated by arrows in A) of the rNCSCs cultured at 0.5% O_2 for 36 hr (A), in contrast with the low expression level of CXCR4 and only background level of HIF1α in the cytoplasm of the rNCSCs cultured at 20%, 40%, and 80% O_2 (B–D). Incubation of the rNCSCs cultured at 0.5% O_2 with the CXCR4-specific antagonist AMD3100 did not affect nuclear expression of HIF1α, but dramatically decreased CXCR4 expression in the nuclei and on the plasma membrane whereas significantly increased CXCR4 expression in the cytoplasm (indicated by arrows in F). The scale bar in A represents 50 μm and applies to panels A–D and F. The statistical histogram in (E) summarizes the percentages of $CXCR4^+$ and $HIF1\alpha^+$ nuclei in the rNCSCs cultured under various oxygen tensions and with different drug treatments (i.e., incubation with AMD3100 or NAC). One-way ANOVA with $n = 12$ was applied, and the hashtags (#) indicate $P < 0.01$. The statistical histograms in (G) and (H) demonstrate that treatment with AMD3100 or transfection with *Cxcr4* or *Hif1α* siRNA significantly decreased the total cell numbers and viability of the rNCSCs cultured at 0.5% O_2 to the levels comparable to those in the rNCSCs cultured at 20% O_2. One-way ANOVA with $n = 12$ in each experimental group was applied, and the asterisk (*) indicates $P < 0.05$, while the hashtags (#) indicate $P < 0.01$.

cultured at 80% O_2 was TP53-independent. It is noteworthy that *TP53* knockdown in the rNCSCs cultured at 80% O_2 did not affect nuclear-to-cytoplasmic translocation of S100A2 whereas greatly increased the cell viability and total numbers of the rNCSCs to the levels comparable with those in the rNCSCs cultured at 20% O_2 ($n = 12$, $P > 0.05$, one-way ANOVA) (Fig. 8G,L).

On the other hand, both the *Tp53 CMV*-transfected rNCSCs cultured at 20% O_2 and the *S100a2* siRNA-transfected rNCSCs cultured at 80% O_2 showed significantly decreased cell viability and total cell numbers in comparison with those in the untreated rNCSCs cultured at 20% O_2 ($n = 12$, $P < 0.01$, one-way ANOVA) (Fig. 8G,L). These results indicated that the level of TP53 expression rather than S100A2 expression or oxygen tensions was the decisive factor for down-regulating cell viability and total numbers of rNCSCs.

Concomitant with the greatly increased nuclear-to-cytoplasmic translocation of S100A2, we also found that the cytoplasmic expression level of TPM1 in the rNCSCs cultured at 80% O_2 was dramatically reduced (indicated by arrows in Fig. 10D) to only averagely 22% of the expression levels in the rNCSCs cultured at 0.5%, 20%, and 40% O_2 ($n = 12$, $P < 0.01$, one-way ANOVA) (Figs. 9C,D, 10A–D). Incubation of the rNCSCs cultured at 80% O_2 with 1 mM of NAC for 36 hr was able to increase cytoplasmic TPM1 expression to the level comparable with that in the untreated rNCSCs cultured at 20% O_2 ($n = 12$, $P > 0.05$, one-way ANOVA) (Figs. 9C,D, 10E). Of interest, *Tp53* overexpression in the *Tp53 CMV*-transfected rNCSCs cultured at 20% O_2 resulted in a TPM1 expression level that was significantly decreased compared with the level in the untreated rNCSCs cultured at 20% O_2 ($n = 12$, $P < 0.05$, one-way ANOVA), whereas significantly increased compared with the level in the untreated rNCSCs cultured at 80% O_2 ($n = 12$, $P < 0.05$, one-way ANOVA) (Figs. 9C,D, 10B,D,G). On the other hand, *TP53* knockdown in the *Tp53* siRNA-transfected rNCSCs cultured at 80% O_2 greatly increased cytoplasmic TPM1 expression to the level comparable with that in the untreated rNCSCs cultured at 20% O_2 ($n = 12$, $P > 0.05$, one-way ANOVA) (Figs. 9C,D, 10B,H). It is noteworthy that *S100a2* siRNA transfection failed to increase TPM1 expression in the rNCSCs cultured at 80% O_2 ($n = 12$, $P < 0.01$ compared with the level in the rNCSCs cultured at 20% O_2, one-way ANOVA) (Figs. 9C,D, 10D,I). Therefore, cytoplasmic TPM1 expression was mainly regulated by TP53 rather than by S100A2 expression.

To further illuminate the regulatory relationship among TP53, TPM1, and S100A2 at the transcriptional level, real-time quantitative reverse transcription polymerase chain reaction (RT-PCR) was performed to analyze the levels of *Tpm1, S100a2*, and *Tp53* mRNA in relation to the *Tbp* mRNA level, which served as an internal normalization control (Fig. 11). Our RT-PCR results

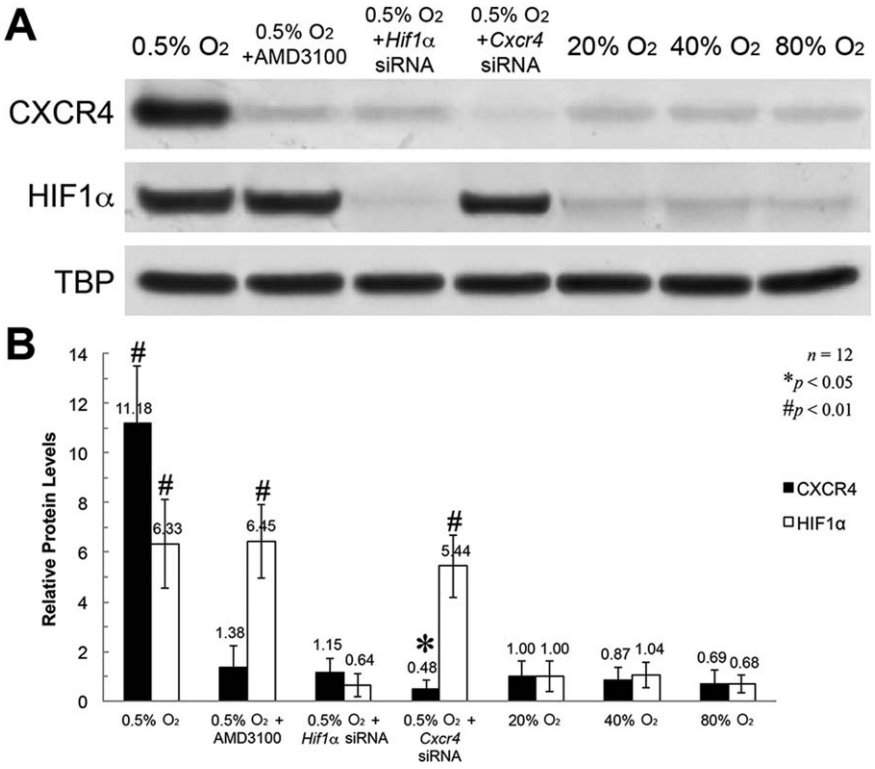

Fig. 6. **A,B**: Significantly decreased nuclear expression of CXCR4 by treatment with AMD3100 or transfection with *Cxcr4* or *Hif1α* siRNA in the rNCSCs cultured at 0.5% O_2 for 36 hr. A: Western blot analyses of nuclear proteins indicated that the expression levels of CXCR4 and HIF1α in the rNCSCs cultured at 0.5% O_2 for 36 hr were, respectively, 11.18 ± 2.34 and 6.33 ± 1.78-fold relative to the levels in the rNCSCs cultured at 20% O_2, which were presumptively set up as 1.0 ($n = 12$, $P < 0.01$, one-way ANOVA). B: On the other hand, the nuclear expression levels of CXCR4 and HIF1α in the rNCSCs cultured at 40% and 80% O_2 for 36 hr (A) were comparable to the levels in the rNCSCs cultured at 20% O_2 ($n = 12$, $P > 0.05$, one-way ANOVA) (B). AMD3100 treatment, *Hif1α* siRNA transfection, and *Cxcr4* siRNA transfection of the rNCSCs cultured at 0.5% O_2, respectively, decreased the nuclear expression levels of CXCR4 to 1.38 ± 0.87, 1.15 ± 0.55, and 0.48 ± 0.36-fold of the level in the rNCSCs cultured at 20% O_2 ($n = 12$, $P > 0.05$ for the levels with AMD3100 treatment and *Hif1α* siRNA transfection and $P < 0.05$ for the level with *Cxcr4* siRNA transfection in comparison with the level at 20% O_2, one-way ANOVA). On the other hand, neither AMD3100 treatment nor *Cxcr4* siRNA transfection significantly decreased the nuclear expression levels of HIF1α in the rNCSCs cultured at 0.5% O_2 for 36 hr (A), which were, respectively, 6.45 ± 1.49 and 5.44 ± 1.26-fold of the level in the rNCSCs cultured at 20% O_2 ($n = 12$, $P < 0.01$, one-way ANOVA) (B). The statistical histogram in (B) represents the quantified relative intensities of the immunoblots shown in (A).

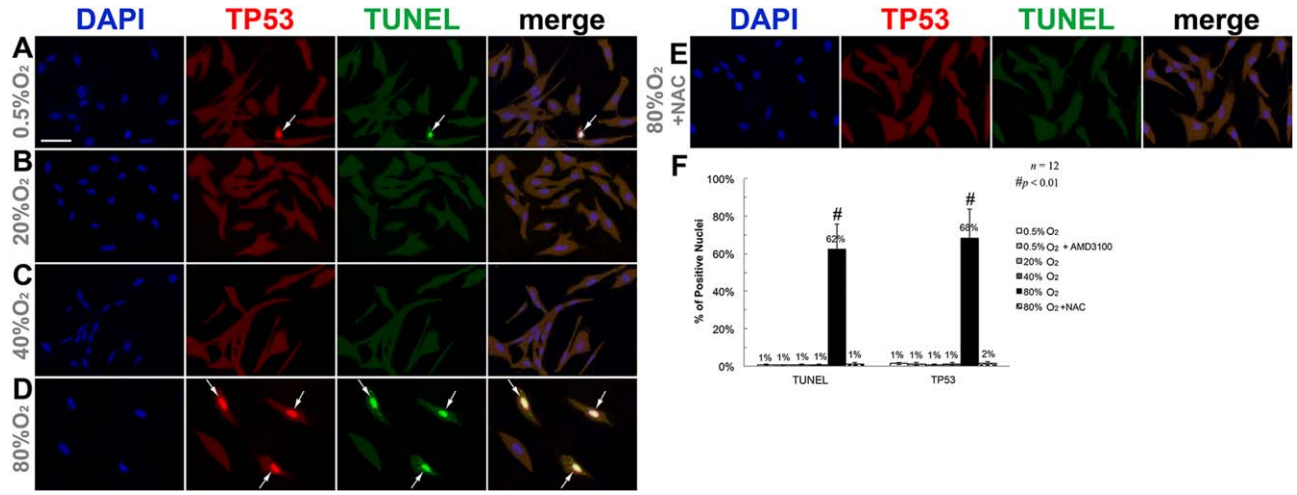

Fig. 7. **A–F**: Significantly increased percentage of $TP53^+$ nuclei was associated with significantly increased apoptosis of the rNCSCs cultured at 80% O_2 for 36 hr. Double immunostaining revealed greatly increased percentages of $TP53^+$ (red) and $TUNEL^+$ (green) nuclei in the rNCSCs cultured at 80% O_2 for 36 hr (D), in comparison with the percentages in the rNCSCs cultured at 0.5%, 20%, and 40% O_2 (A–C) ($n = 12$, $P < 0.01$, one-way ANOVA). Incubation with NAC at 80% O_2 significantly decreased apoptosis of the rNCSCs to the level comparable to that in the rNCSCs cultured at 20% or 40% O_2 ($n = 12$, $P > 0.05$, one-way ANOVA) (compare panel E with panels B and C). The scale bar in A represents 50 μm and applies to panels A–E. F: The statistical histogram summarizes the percentages of $TUNEL^+$ and $TP53^+$ nuclei in the rNCSCs cultured under various oxygen tensions and with different drug treatments. One-way ANOVA with $n = 12$ was applied, and the hashtags (#) indicate $P < 0.01$.

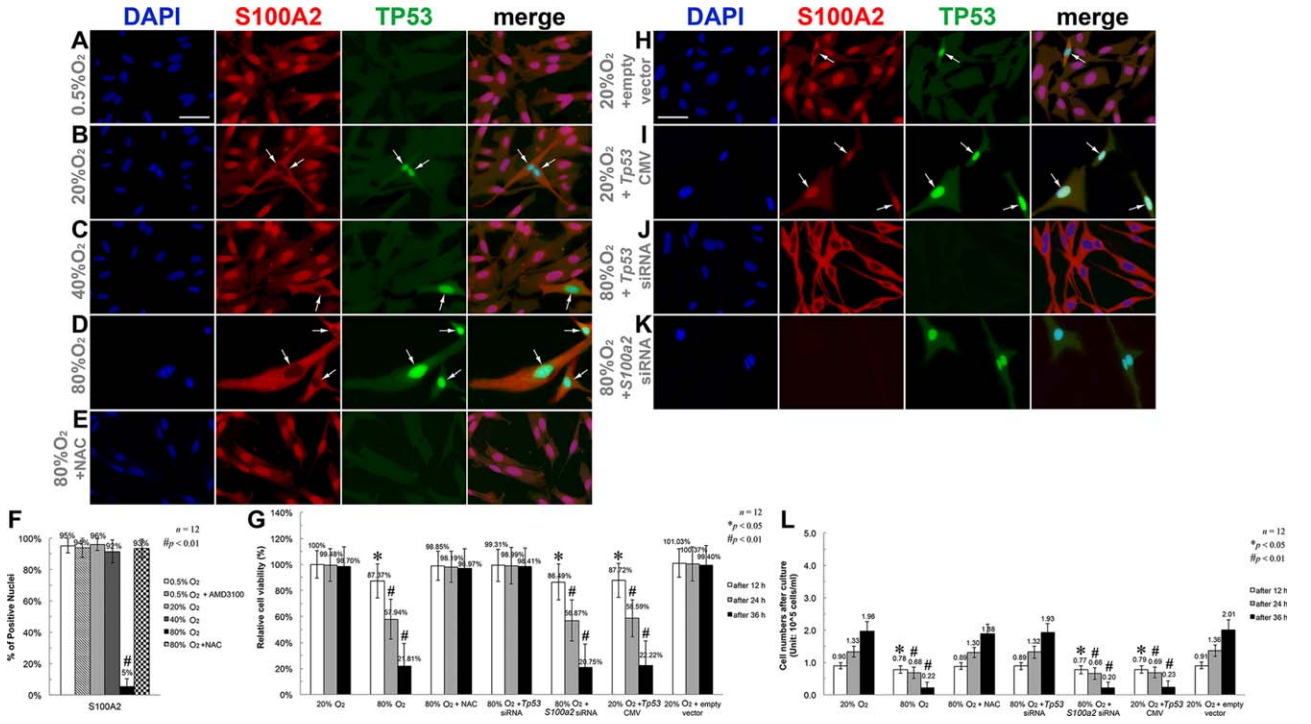

Fig. 8. **A–L**: Dramatically increased nuclear-to-cytoplasmic translocation of S100A2 in the rNCSCs cultured at 80% O_2 was independent of TP53 expression. Double immunostaining revealed dramatically increased expression levels of cytoplasmic S100A2 (red) and nuclear TP53 (green) in the rNCSCs cultured at 80% O_2 for 36 hr (D), in comparison with the levels in the rNCSCs cultured at 0.5%, 20%, and 40% O_2 (A–C) (see also Fig. 9). While cultured without any drug treatment or gene transfection at 20%, 40%, and 80% O_2, the rNCSCs that showed strong cytoplasmic and weak nuclear expression of S100A2 always displayed strong nuclear expression of TP53 (indicated by arrows in panels B–D). Incubation with NAC at 80% O_2 dramatically suppressed nuclear-to-cytoplasmic translocation of S100A2 and decreased nuclear expression of TP53 to the levels comparable to those in the rNCSCs cultured at 0.5%, 20%, and 40% O_2 (compare panel E with panels A–C). The scale bar in A represents 50 μm and applies to panels A–E. The statistical histogram in (F) demonstrates a dramatically reduced percentage of $S100A2^+$ nuclei in the rNCSCs cultured at 80% O_2 in comparison with the high percentages (>90%) in the rNCSCs cultured at 0.5%, 20% and 40% O_2 as well as the NAC-treated rNCSCs cultured at 80% O_2 ($n = 12$, $P < 0.01$, one-way ANOVA). Of interest, after transfection with a rat *Tp53*-expressing vector (*Tp53 CMV*), the rNCSCs cultured at 20% O_2 showed dramatically increased nuclear expression of TP53 and colocalization of TP53 and S100A2 in the nuclei, without increased nuclear-to-cytoplasmic translocation of S100A2 (indicated by arrows in panel I). On the other hand, inhibition of TP53 expression in the rNCSCs cultured at 80% O_2 by *Tp53* siRNA transfection did not influence the dramatically increased nuclear-to-cytoplasmic translocation of S100A2 (J). And *vice versa*, inhibition of S100A2 expression in the rNCSCs cultured at 80% O_2 by *S100a2* siRNA transfection did not influence the dramatically increased nuclear expression of TP53 (K). The scale bar in H represents 50 μm and applies to panels H–K. The statistical histograms in (G) and (L) demonstrate that treatment with NAC or transfection with *Tp53* siRNA significantly increased the cell viability and total numbers of the rNCSCs cultured at 80% O_2 to the levels comparable to those in the rNCSCs cultured at 20% O_2 ($n = 12$, $P > 0.05$, one-way ANOVA). On the other hand, transfection with *S100a2* siRNA did not increase the cell viability and total numbers of the rNCSCs cultured at 80% O_2 ($n = 12$, $P < 0.05$ after 12 hr of culturing and $P < 0.01$ after 24 and 36 hr of culturing in comparison with the levels in the rNCSCs cultured at 20% O_2, one-way ANOVA), while transfection with the *Tp53 CMV* vector significantly decreased the cell viability and total numbers of the rNCSCs cultured at 20% O_2 to the levels comparable with those in the rNCSCs cultured at 80% O_2 ($n = 12$, $P < 0.05$ after 12 hr of culturing and $P < 0.01$ after 24 and 36 hr of culturing in comparison with the levels in the rNCSCs cultured at 20% O_2, one-way ANOVA). One-way ANOVA with $n = 12$ in each experimental group was applied, and the asterisks (*) indicate $P < 0.05$, while the hashtags (#) indicate $P < 0.01$.

showed relatively constant expression levels of *S100a2* mRNA in rNCSCs cultured under different oxygen tensions (Fig. 11A,B), indicating that S100A2 translocation rather than transcription was subject to regulation by the increased oxygen tension. On the other hand, *Tpm1* expression was significantly decreased when *Tp53* expression was significantly increased, and *vice versa*, no matter under normoxia (i.e., decreased *Tpm1* expression in the *Tp53*-overexpressing rNCSCs) or hyperoxia (i.e., increased *Tpm1* expression in the *Tp53*-knockdown rNCSCs), indicating that the *Tpm1* mRNA level was down-regulated by TP53, either directly or indirectly.

Of interest, however, the level of *Tpm1* mRNA in the *Tp53*-overexpressing rNCSCs cultured at 20% O_2 was significantly higher than the levels in the untreated and *S100a2* siRNA-transfected rNCSCs cultured at 80% O_2, which expressed lower levels of *Tp53* mRNA (Fig. 11A,B). This result indicated that the inhibitory effect of TP53 on *Tpm1* expression in the rNCSCs was weaker under normoxia and stronger under hyperoxia, and it is likely that other protein(s) or factor(s) may participate in regulating the inhibitory capability of TP53 under different oxygen tensions.

Previous studies have demonstrated that S100A2 may compete with F-actin for binding to tropomyosins in microvilli in the cytoplasm of LLC PK1 cells (Gimona et al., 1997), and cell stretching/extension was significantly reduced by treatment with HIF1α-stabilizing chemical compounds (Scully et al., 2016). Because we observed significantly increased HIF1α expression in the rNCSCs cultured at 0.5% O_2 (Figs. (5 and 6)) as well as increased nuclear-to-cytoplasmic translocation of S100A2 and significantly decreased TPM1 expression in the rNCSCs cultured

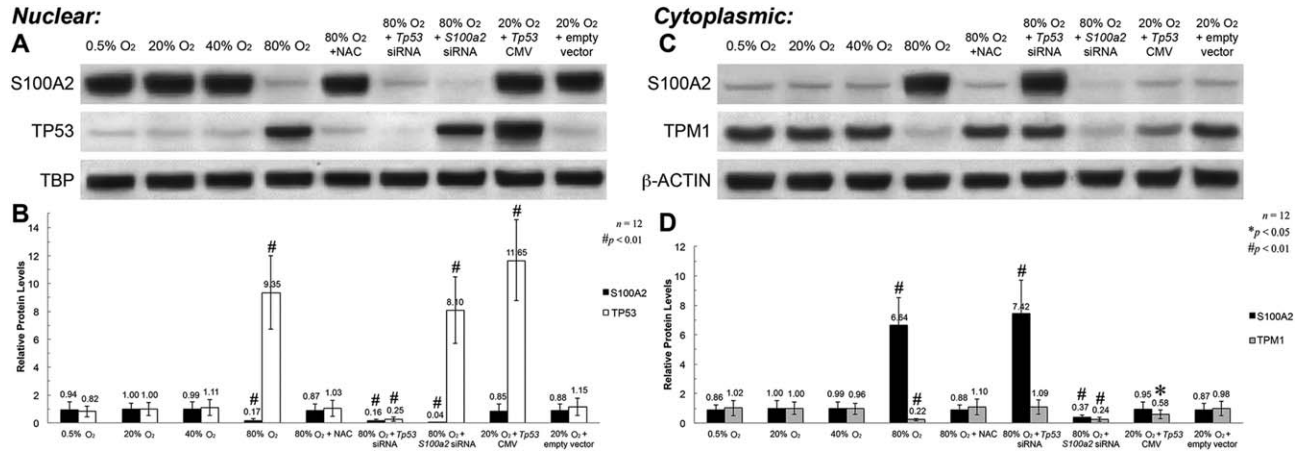

Fig. 9. **A–D**: Subcellular expression analyses demonstrated hyperoxia-dependent and TP53-independent nuclear-to-cytoplasmic translocation of S100A2 as well as TP53 dose-dependent regulation of cytoplasmic TPM1 expression in rNCSCs. A,B: Western blot analyses indicated that the nuclear expression levels of S100A2 in both the untreated and *Tp53* siRNA-transfected rNCSCs cultured at 80% O_2 were significantly decreased to less than 20% of the levels in the rNCSCs cultured at 20% O_2, which were presumptively set up as 1.0 ($n = 12$, $P < 0.01$, one-way ANOVA), while the nuclear expression level of S100A2 in the *Tp53 CMV*-transfected rNCSCs cultured at 20% O_2 was comparable with the level in the rNCSCs cultured at 20% O_2 ($n = 12$, $P > 0.05$, one-way ANOVA). C,D: Similarly, the cytoplasmic expression levels of S100A2 in the rNCSCs cultured at 80% and 20% O_2 were unaffected by transfection with *Tp53* siRNA and *Tp53 CMV*, respectively ($n = 12$, $P < 0.01$ for the *Tp53* siRNA-transfected rNCSCs cultured at 80% O_2 and $P > 0.05$ for the *Tp53 CMV*-transfected rNCSCs cultured at 20% O_2, in comparison with the expression levels in the rNCSCs cultured at 20% O_2, one-way ANOVA). It is noteworthy that the *S100a2* siRNA-transfected rNCSCs cultured at 80% O_2 also expressed nuclear TP53 at a level comparable to that in the untreated rNCSCs cultured at 80% O_2 ($n = 12$, $P < 0.01$ compared with the level in the rNCSCs cultured at 20% O_2, one-way ANOVA) (A,B). Therefore, the expression levels of S100A2 and TP53 are independent of each other. On the other hand, the cytoplasmic expression level of TPM1 in the *Tp53* siRNA-transfected rNCSCs cultured at 80% O_2 was significantly higher than the level in the untreated rNCSCs cultured at 80% O_2 and comparable with the level in the rNCSCs cultured at 20% O_2 ($n = 12$, $P > 0.05$, one-way ANOVA) (C,D). In addition, the expression level of TPM1 in the *Tp53 CMV*-transfected rNCSCs cultured at 20% O_2 was higher than the level in the untreated rNCSCs cultured at 80% O_2 whereas significantly lower than the level in the rNCSCs cultured at 20% O_2 ($n = 12$, $P < 0.01$, one-way ANOVA) (C,D). Of interest, the *S100a2* siRNA-transfected rNCSCs cultured at 80% O_2 expressed cytoplasmic TPM1 at a level comparable to that in the untreated rNCSCs cultured at 80% O_2 ($n = 12$, $P < 0.01$ compared with the level in the rNCSCs cultured at 20% O_2, one-way ANOVA) (C,D). Therefore, the expression level of TPM1 is dependent on the nuclear level of TP53 but independent of the expression level of S100A2. In contrast to the limited effects of gene knockdown on merely one or two specific genes, NAC treatment was able to simultaneously down-regulate S100A2 translocation and TP53 expression as well as up-regulate TPM1 expression ($n = 12$, $P > 0.05$ compared with the level in the rNCSCs cultured at 20% O_2, one-way ANOVA) (A–D). The statistical histograms in (B) and (D) represent the quantified relative intensities of the immunoblots shown in (A) and (C), respectively.

at 80% O_2 (Figs. 9–11), it was of interest to analyze whether F-actin expression and organization as well as the cell stretch length were affected in the rNCSCs cultured under hypoxia or hyperoxia. Double staining with phalloidin and anti-cortactin (CTTN) antibody revealed that, among the rNCSCs cultured at 0.5%, 20%, 40%, and 80% O_2, both F-actin and cortactin showed comparable expression levels and patterns (Fig. 12A–D), and the cell stretch length did not show significant differences among distinct oxygen tensions, despite slightly increased average stretch lengths at 40% and 80% O_2 ($n = 600$, $P > 0.05$, one-way ANOVA) (Fig. 12E). Our results demonstrate that neither polymerization of actin nor extension/elongation of rNCSCs was significantly influenced by extreme oxygen tensions.

Discussion

The results of our study demonstrate that two extreme oxygen tensions, 0.5% and 80% O_2, differentially up-regulate and down-regulate rNCSC proliferation and viability via regulatory pathways consisting respectively of the HIF1α–CXCR4 and TP53–TPM1 proteins (summarized in Fig. 13). Our results demonstrate that 0.5% O_2 increases proliferation of rNCSCs but not rMSCs, which even showed significantly decreased cell viability and total cell numbers at 0.5% O_2 (Fig. 2), indicating that hypoxia-induced proliferation is cell type-specific. On the other hand, our results demonstrate that 80% O_2 decreases cell viability and proliferation of rNCSCs but not rMSCs, which showed barely changed cell viability and total cell numbers at 80% O_2 (Fig. 2), indicating that the inhibitory effect of hyperoxia on cell viability and proliferation is also cell type-specific. In fact, previous studies have shown that hypoxia exposure decreases proliferation and viability of both human and rat MSCs (Holzwarth et al., 2010; Saini et al., 2013), and hyperoxia (100% O_2) preconditioning before hypoxia exposure significantly increases the proliferation and survival rates of the rMSCs (Saini et al., 2013).

Of interest, it was reported that cleavage of the intracellular domain of NGFR (p75) under hypoxia was required for HIF1α stabilization in mouse fibroblasts and cerebellar granule neurons (Le Moan et al., 2011). However, despite the significantly increased nuclear expression of HIF1α proteins in the rNCSCs cultured at 0.5% O_2, we did not observe an increased expression level of NGFR in the cytoplasm or nuclei of the rNCSCs cultured at 0.5% O_2 compared with the level in the rNCSCs cultured at 20% O_2 (Fig. 1A–D). The percentages of the rNCSCs showing strong nuclear expression of NGFR were also comparable among the rNCSCs cultured under various oxygen tensions (see also the Results section). Previous studies also demonstrated a predominantly cytoplasmic and partially nuclear expression pattern of NGFR in NCSCs (Wong et al., 2006; Lee et al., 2007; Kerosuo et al., 2015). It is likely that the HIF1α protein level in rNCSCs is

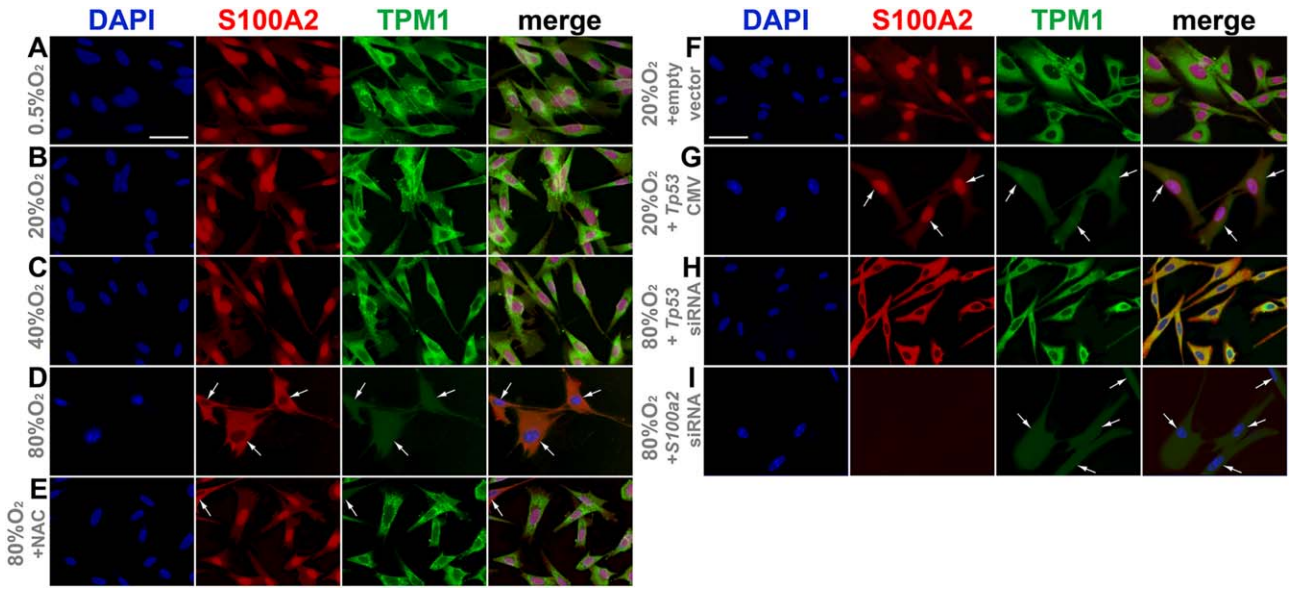

Fig. 10. A–I: Dramatically decreased cytoplasmic expression of TPM1 in the rNCSCs cultured at 80% O_2 was independent of S100A2 expression but dependent on TP53 expression levels. Double immunostaining revealed significantly increased cytoplasmic expression of S100A2 (red) whereas dramatically decreased cytoplasmic expression of TPM1 (green) in the rNCSCs cultured at 80% O_2 for 36 hr (indicated by arrows in D), in comparison with the expression levels in the rNCSCs cultured at 0.5%, 20%, and 40% O_2 (A–C). TPM1 showed predominantly perinuclear expression in the cytoplasm of the rNCSCs cultured at 0.5%, 20%, and 40% O_2 (A–C), whereas displayed only a background immunostaining level throughout the whole cell in the rNCSCs cultured at 80% O_2 (D). Incubation with NAC at 80% O_2 dramatically suppressed nuclear-to-cytoplasmic translocation of S100A2 and increased cytoplasmic expression of TPM1 to the levels comparable to those in the rNCSCs cultured at 0.5%, 20%, and 40% O_2 (compare panel E with panels A–C). The scale bar in A represents 50 μm and applies to panels A–E. Of interest, the cytoplasmic TPM1 expression level in the *Tp53 CMV*-transfected rNCSCs cultured at 20% O_2, which expressed S100A2 predominantly in the nuclei, was significantly decreased in comparison with the TPM1 level in the untreated rNCSCs cultured at 20% O_2 (indicated by arrows in G, and compare between panels B and G). Therefore, increased TP53 expression was sufficient to significantly decrease TPM1 expression in rNCSCs under normoxia. On the other hand, the *Tp53* siRNA-transfected rNCSCs cultured at 80% O_2, which showed predominantly cytoplasmic expression of S100A2, expressed cytoplasmic TPM1 at a level comparable to those in the rNCSCs cultured at 0.5%, 20%, and 40% O_2 (compare panel H with panels A–C). It is noteworthy that the cytoplasmic TPM1 expression level in the *S100a2* siRNA-transfected rNCSCs cultured at 80% O_2 was as low as the level in the untreated rNCSCs cultured at 80% O_2, indicating that TPM1 expression was not subject to regulation by S100A2. The scale bar in F represents 50 μm and applies to panels F–I.

mainly regulated by protein factors other than NGFR and Siah2, so that the increased HIF1α level is not correlated with an increased intracellular level of NGFR in the rNCSCs cultured at 0.5% O_2. It remains to be studied whether there are other protein factors in rNCSCs that down-regulate prolyl hydroxylase or asparagine hydroxylase and up-regulate HIF1α stabilization in response to hypoxia exposure.

Another neural crest marker, SNAIL, has been shown to be a direct target of HIF1α in mediating EMT in various types of cancer cells. However, in rNCSCs cultured at 0.5% O_2, we failed to detect significant changes of SNAIL expression in the presence of dramatically increased nuclear expression of HIF1α (Figs. 1I, 5A,E, 6). Of interest, previous studies have demonstrated that the regulatory relationship between HIF1α and SNAIL may be dependent on species and cell types (Barriga et al., 2013; Scully et al., 2016), as inhibition of HIF1α expression by morpholino injection did not affect *Snail1* and *Snail2* expression in neural crest cells of the *Xenopus laevis* embryos (Barriga et al., 2013), whereas HIF1α stabilization increased *SNAIL2* expression in cranial neural crest cells of the chick embryos (Scully et al., 2016).

It has also been demonstrated that *Cxcr4* and *Twist* instead of *Snail1* and *Snail2* are the major *Hif1α* target genes regulating EMT of *Xenopus* neural crest (Barriga et al., 2013). In agreement with the previous study (Barriga et al., 2013), in rat neural crest cells we also found that CXCR4 instead of SNAIL was a major HIF1α target gene (Figs. 1I, 5A,E, 6). It is likely that, while the HIF1α-SNAIL is a major regulatory pathway promoting EMT of cancer cells in the pathological environment, the HIF1α-CXCR4 or HIF1α-TWIST pathways are predominant in regulating EMT of *Xenopus* and rat neural crest cells in the native environment (Barriga et al., 2013).

It was previously reported that, under normoxia, hair follicles in the normal rat skin were not labeled with hypoxyprobe-1, whereas plenty of hypoxyprobe-1^+ signals were present in the hair follicles and newly formed epidermis in the incisionally wounded rat skin for 3 weeks after wounding (Lokmic et al., 2006). In agreement with the previous study, we demonstrated no hypoxyprobe-1 staining signal in the whisker hair follicles of the Sprague-Dawley rats exposed to normoxia (Fig. 3A), while there were dramatically increased hypoxyprobe-1^+ signals in association with significantly increased percentages of $SOX10^+$ and $BrdU^+$ cells in the rat hair follicles exposed to hypoxia (Fig. 3A–C). It was also shown in the previous study that cell proliferation rates were significantly increased in the wounded skin tissue compared with normal skin during the wound healing process (Lokmic et al., 2006). Our results further associate increased proliferation and total numbers of $SOX10^+$ rNCSCs with the hypoxic hair follicles in vivo, and may provide explanation for the molecular mechanisms underlying hair follicle regeneration in the wounded skin.

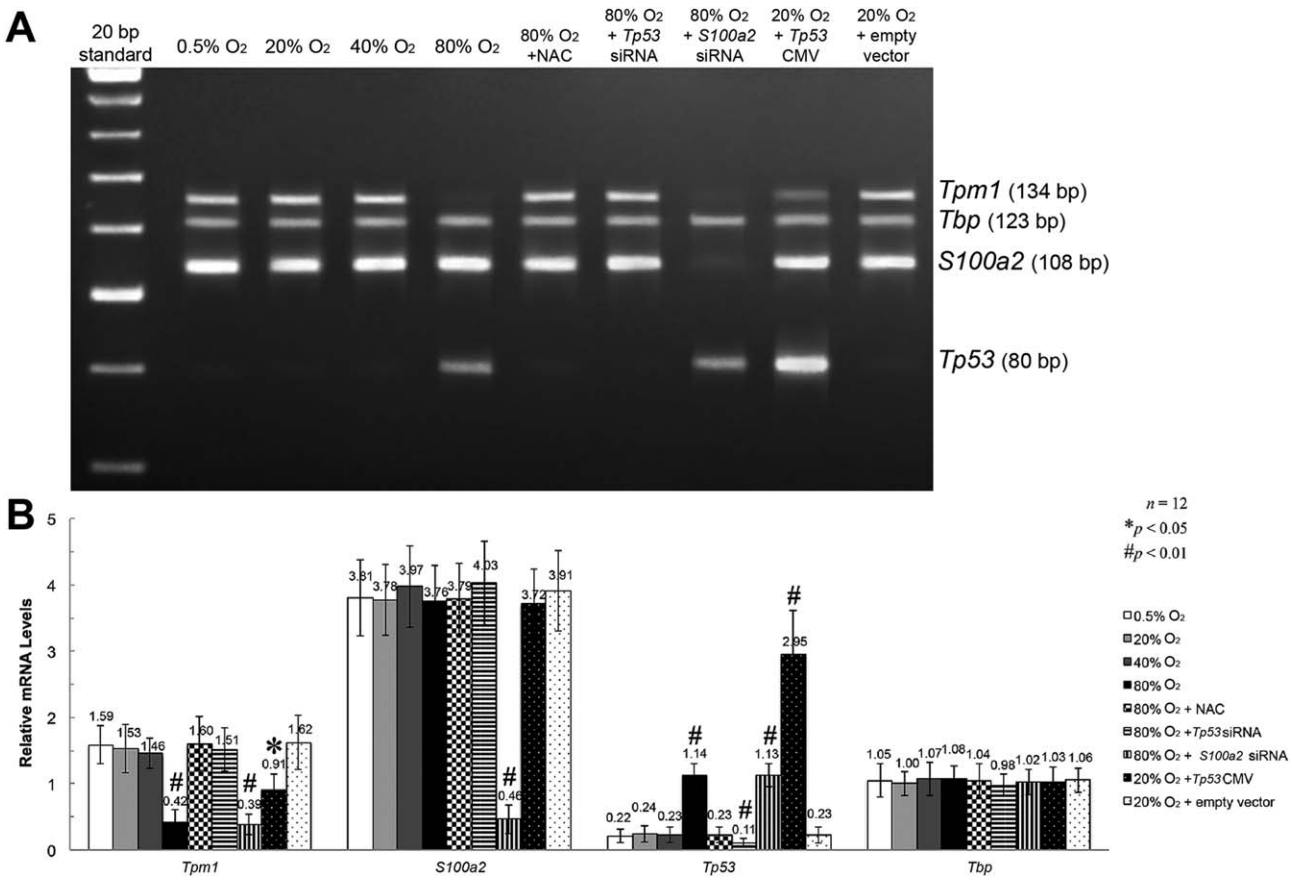

Fig. 11. Unchanged *S100a2* mRNA levels in rNCSCs cultured under various oxygen tensions, and dramatically increased *Tp53* and decreased *Tpm1* mRNA levels in the rNCSCs cultured at 80% O_2. **A**: Real-time quantitative RT-PCR indicated comparable levels of *S100a2* mRNA among the rNCSCs cultured at 0.5%, 20%, 40%, and 80% O_2 ($n = 12$, $P > 0.05$, one-way ANOVA), whereas dramatically decreased *Tpm1* and increased *Tp53* mRNA levels in the rNCSCs cultured at 80% O_2 compared with the levels in the rNCSCs cultured at 0.5%, 20%, and 40% O_2 ($n = 12$, $P < 0.01$, one-way ANOVA). NAC treatment of the rNCSCs cultured at 80% O_2 significantly increased *Tpm1* and decreased *Tp53* mRNA expression to the levels comparable with those in the rNCSCs cultured at 20% O_2 ($n = 12$, $P > 0.05$, one-way ANOVA). Of interest, while *Tp53* siRNA transfection significantly increased *Tpm1* mRNA expression to the level comparable with that in the rNCSCs cultured under normoxia ($n = 12$, $P > 0.05$, one-way ANOVA), *S100a2* siRNA transfection failed to increase *Tpm1* and decrease *Tp53* mRNA levels in the rNCSCs cultured at 80% O_2 ($n = 12$, $P < 0.01$ in comparison with the levels in the rNCSCs cultured at 20% O_2, one-way ANOVA). It is noteworthy that *Tp53 CMV* transfection in the rNCSCs cultured at 20% O_2 dramatically increased *Tp53* mRNA level to be more than two folds of the level in the rNCSCs cultured at 80% O_2 (see also panel B) ($n = 12$, $P < 0.01$, one-way ANOVA), whereas the *Tpm1* mRNA level in the rNCSCs with *Tp53* overexpression was still significantly lower than the level in the rNCSCs without *Tp53* overexpression under normoxia (see also panel B) ($n = 12$, $P < 0.05$, one-way ANOVA). **B**: The relative mRNA levels of *Tpm1, Tbp, S100a2*, and *Tp53* were quantitated and are shown in the histogram, with the *Tbp* mRNA level in the rNCSCs cultured at 20% O_2 presumptively set up as 1.0. One-way ANOVA with $n = 12$ in each experimental group was applied, and the asterisks (*) indicate $P < 0.05$, while the hashtags (#) indicate $P < 0.01$.

Previous studies have demonstrated that, in addition to regulating neural crest cell migration, the endogenous chemokine SDF-1/CXCL12 and its receptor CXCR4 are also implicated in promoting proliferation of neural crest stem/progenitor cells in both mouse hair follicles and chick embryos (Belmadani et al., 2009; Rezzoug et al., 2011). In addition, both HIF1α and CXCR4 have been shown to up-regulate proliferation of various types of stem/progenitor cells and carcinoma cells (Carmeliet et al., 1998; Goda et al., 2003; Kahn et al., 2004; do Carmo et al., 2010; Heckmann et al., 2013; Nombela-Arrieta et al., 2013; Park et al., 2013; Shen et al., 2013; Guo et al., 2014; Xia et al., 2014; Guan et al., 2015; Guimaraes-Camboa et al., 2015; Liu et al., 2015; Zhang et al., 2015). Nuclear expression of HIF1α or CXCR4 has been frequently detected in carcinoma cells and associated with metastasis and poor prognosis of cancers (Moroz et al., 2009; Speetjens et al., 2009; Wang et al., 2009; Darekar et al., 2012; Don-Salu-Hewage et al., 2013; Deb et al., 2014).

Interestingly, the roles of HIF1α and CXCR4 in regulating cell proliferation were contradictory among distinct types of stem/progenitor cells. It has been demonstrated that HIF1α induced apoptosis and suppressed proliferation of embryonic stem cells but reduced apoptosis and enhanced proliferation of mesenchymal stem cells and hypoxic fetal cardiomyocytes (Carmeliet et al., 1998; Li and Zhang, 2010; Guimaraes-Camboa et al., 2015; Kakudo et al., 2015). CXCR4 has been shown to inhibit proliferation of hematopoietic stem cells whereas promote proliferation of fetal pancreatic endocrine progenitor cells, endothelial cells, tracheal epithelial cells, and normal pituitary cells (Lee et al., 2008b; Nie et al., 2008; Kayali et al., 2012; Liu et al., 2013; Noels et al., 2014). Nuclear localization of HIF1α has been reported in embryonic and hematopoietic stem cells to regulate respectively their

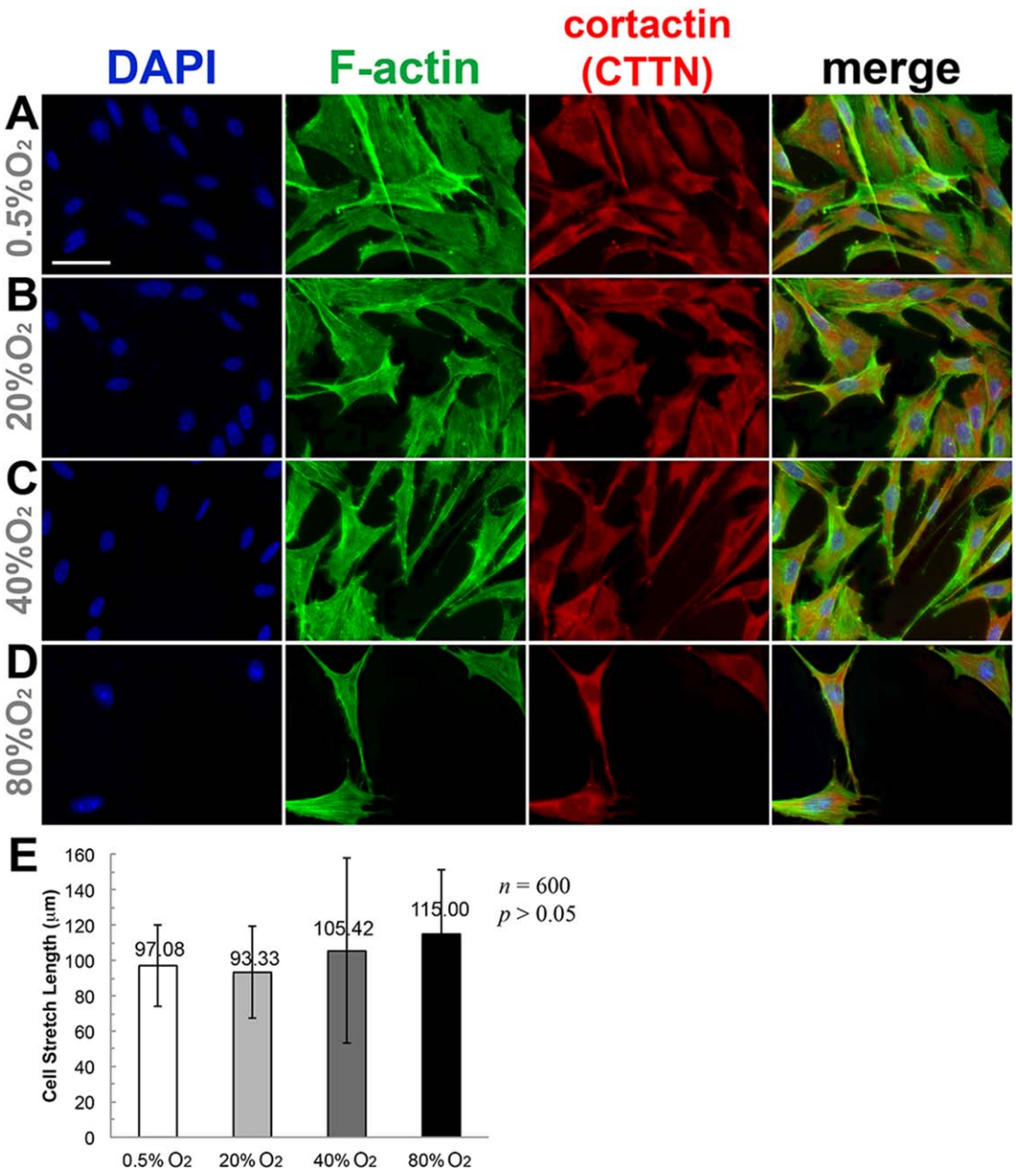

Fig. 12. **A–E**: Normal expression and organization of F-actin and cortactin as well as unaffected cell stretch lengths in rNCSCs cultured under various oxygen tensions. Double staining with phalloidin and anti-cortactin (CTTN) antibody revealed comparable expression levels and patterns of F-actin (green) and cortactin (red) in the cytoplasm among the rNCSCs cultured at 0.5% (A), 20% (B), 40% (C), and 80% O_2 (D) for 36 hr. While F-actin was detected in microfilaments spanning throughout the whole cells, cortactin was expressed more strongly in the cytoplasm compared with the nuclei. The scale bar in A represents 50 μm and applies to panels A–D. The statistical histogram in (E) shows the average lengths of the longest axes of individual rNCSCs cultured under various oxygen tensions, with totally 600 cells from 6 independent experiments were measured for each oxygen level ($P > 0.05$ by one-way ANOVA).

pluripotency and cell cycle quiescence (Forristal et al., 2010; Takubo et al., 2010). Nuclear localization of CXCR4 has also been reported in fetal mesenchymal stem cells and is regulated by intracellular trafficking (Pelekanos et al., 2014).

While the HIF1α-CXCR4 regulatory pathway has been shown to play a major role in regulating EMT of neural crest cells in vivo (Staller et al., 2003; Rezzoug et al., 2011; Barriga et al., 2013; Escot et al., 2013), our results further identified an indispensible role of the HIF1α-CXCR4 regulatory pathway in promoting rNCSC proliferation under hypoxia (0.5% O_2) in vitro (Figs. 4–6). Of interest, while increased HIF1α stabilization was shown to decrease in vitro proliferation and elongation/extension of the cranial neural crest cells extracted from chick embryos (Scully et al., 2016), in the NCSCs extracted from adult rat whisker hair follicles we observed significantly increased proliferation in association with increased nuclear HIF1α expression, as well as unaffected cell elongation/extension under hypoxia (Figs. 4–6 and 12). In addition, neural crest cells in the adult rat whisker hair follicles exposed to hypoxia also demonstrated significantly increased proliferation and total cell numbers (Fig. 3). Therefore,

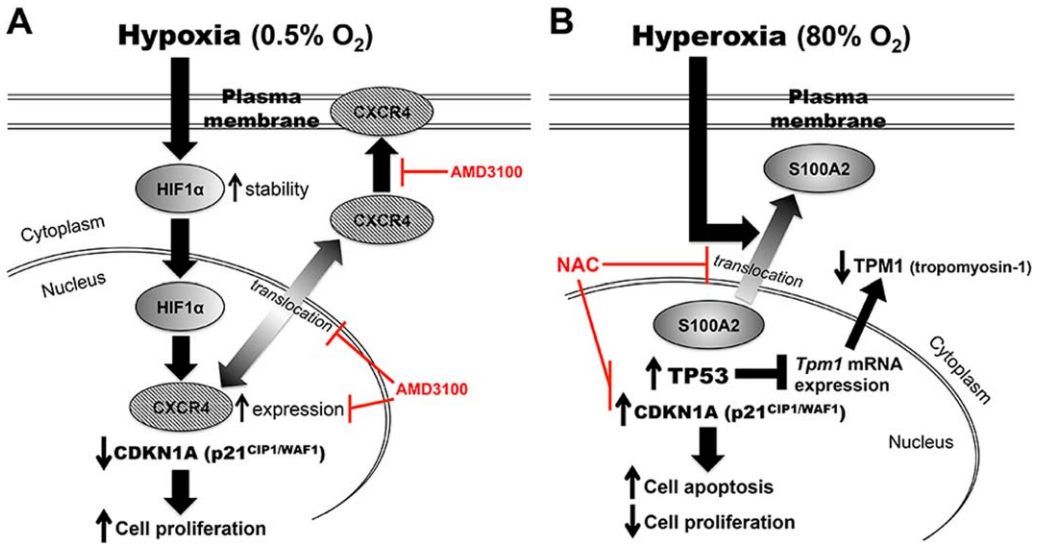

Fig. 13. **A,B**: Schematic illustration of the two distinct regulatory pathways that differentially control rNCSC proliferation and viability under hypoxia (at 0.5% O_2) and hyperoxia (at 80% O_2). Our findings demonstrate that, under hypoxia (at 0.5% O_2) (A), increased nuclear expression of HIF1α is associated with increased expression and/or translocation of CXCR4 to the nuclei and plasma membranes of the rNCSCs. The increased expression level of CXCR4 in the nuclei is concomitant with decreased nuclear expression of the cyclin-dependent kinase inhibitor CDKN1A ($p21^{CIP1/WAF1}$) and increased proliferation of the rNCSCs. Incubation of the rNCSCs cultured under hypoxia with the CXCR4-specific antagonist AMD3100 suppresses translocation of CXCR4 to the plasma membranes and nuclei as well as inhibits CXCR4 expression in the nuclei, leading to decreased proliferation of the rNCSCs. On the other hand, hyperoxia at 80% O_2 (B) increases nuclear-to-cytoplasmic translocation of S100A2 and nuclear expression of TP53, which decreases the mRNA level of *Tpm1* in rNCSCs. The increased expression level of TP53 in the nuclei is concomitant with increased nuclear expression of CDKN1A, increased apoptosis and decreased proliferation of the rNCSCs. Incubation of the rNCSCs cultured at 80% O_2 with the antioxidant *N*-acetylcysteine (NAC) suppresses nuclear-to-cytoplasmic translocation of S100A2, increases cytoplasmic expression of TPM1, and decreases nuclear expression of TP53 and CDKN1A, leading to decreased apoptosis and increased proliferation of the rNCSCs.

hypoxia-dependent or HIF1α-dependent regulation of neural crest cell proliferation and extension may be species-specific, and may be different between embryonic and adult tissues.

It is noteworthy that inhibition of nuclear translocation and/or expression of CXCR4 by AMD3100 treatment or *Cxcr4* siRNA transfection did not alter nuclear expression of HIF1α but was sufficient to decrease proliferation of the rNCSCs cultured at 0.5% O_2 to the level comparable to that in the rNCSCs cultured at 20% O_2 (Figs. 4–6). On the other hand, *Hif1α* siRNA transfection caused not only dramatically reduced HIF1α expression but also significantly decreased CXCR4 expression in the nuclei of the rNCSCs cultured at 0.5% O_2 (Fig. 6). These results indicated that CXCR4 was downstream of HIF1α in up-regulating rNCSC proliferation. In fact, previous studies have demonstrated that HIF1α binds directly to the hypoxia response element on the *CXCR4* promoter and thereby up-regulates *CXCR4* expression in endothelial cells and various carcinoma cells (Schioppa et al., 2003; Staller et al., 2003; Liu et al., 2006; Ishikawa et al., 2009; Melchionna et al., 2010; Luczak et al., 2012; Guo et al., 2014; Suzuki et al., 2014; Guan et al., 2015). In addition, a recent study showed that HIF1α up-regulated proliferation of neuroblastoma cells, which were derived from neural crest progenitor cells, via the sonic hedgehog (SHH) signaling pathway (Chen et al., 2015). Here our study demonstrates for the first time that CXCR4 plays an indispensible role in the HIF1α-induced up-regulation of NCSC proliferation under hypoxia.

In contrast to the HIF1α-dependent stimulatory effect of hypoxia (0.5% O_2) on rNCSCs, our findings identified TP53 as the critical transcription factor mediating the inhibitory effect of a sublethal level of hyperoxia as high as 80% O_2 on rNCSCs (Fig. 13). Although 80% O_2 up-regulated both the nuclear expression of TP53 and nuclear-to-cytoplasmic translocation of S100A2 in rNCSCs, the inhibitory effect of hyperoxia on rNCSC proliferation was prevented by transfection with *Tp53* siRNA rather than *S100a2* siRNA (Fig. 8G,L), and overexpression of *Tp53* alone in the rNCSCs cultured at 20% O_2 was sufficient to recapitulate the inhibitory effect of 80% O_2 on rNCSC viability (Fig. 8G,L), indicating that TP53 instead of S100A2 was the key mediator of hyperoxia-induced inhibition of rNCSC proliferation. Of interest, a previous study reported that, in human osteogenic sarcoma cell lines, S100A2 was transcriptionally activated by TP53, which bound directly to the *S100a2* promoter (Tan et al., 1999). Nonetheless, our results demonstrate unchanged levels of *S100a2* mRNA in rNCSCs cultured under different oxygen tensions, even in the presence of a dramatically increased *Tp53* mRNA level at 80% O_2 (Fig. 11). Our findings indicate that, in rNCSCs, TP53 rather than S100A2 is transcriptionally up-regulated by hyperoxia (80% O_2) (Fig. 11), and hyperoxia regulates S100A2 post-translationally by altering its subcellular localization, namely, promoting its nuclear-to-cytoplasmic translocation (Figs. 8–10).

While a previous study demonstrated that S100A2 might modulate the organization of the actin cytoskeleton via forming 1:1 crosslinking complexes with tropomyosin chains and preventing tropomyosin from binding to F-actin bundles in the cytoplasmic microvilli of the LLC PK1 cells (Gimona et al., 1997), in rNCSCs cultured at 80% O_2,we observed normal actin organization (Fig. 12) and a dramatically reduced mRNA level of *Tpm1* due to increased *TP53* expression instead of altered *S100A2* expression

(Fig. 11). Our results indicate that TPM1 is down-regulated by TP53 at the mRNA level; hence, the expression levels of both *Tp53* and *Tpm1* are hyperoxia-dependent in rNCSCs, while neither *S100a2* expression nor actin organization in rNCSCs is dependent on oxygen tensions.

Of interest, in the *Tp53*-overexpressing rNCSCs cultured at 20% O_2, the expression level of *Tpm1* mRNA was even higher than the level in the rNCSCs cultured at 80% O_2 (Fig. 11), indicating that the reduction of the *Tpm1* mRNA level is not simply proportional to the increase of the *Tp53* mRNA level. It is likely that the gene-regulatory activity of TP53 is further regulated by S100A2, as both TP53 and S100A2 were colocalized in the nuclei of the *Tp53*-overexpressing rNCSCs cultured at 20% O_2, and S100A2 has been reported to modulate both the DNA-binding and transcriptional activities of TP53 in a Ca^{2+}-dependent manner (Mueller et al., 2005). Further studies will be required to illuminate the role of S100A2 in modulating the transcriptional or posttranscriptional regulation of TPM1 by TP53.

Interestingly, previous studies have reported that TPM1 is subject to phosphorylation and plays a key role in cytoskeleton remodeling and stress fiber formation in response to oxidative stress (Houle et al., 2003, 2007), and the oxidative stress-promoted formation of disulfide cross-bridges in TPM1 is associated with an increased TNF-α expression level and impaired myocardial contractile function (Canton et al., 2006). On the other hand, there have been recent studies showing that TPM1 functions as a tumor-suppressor gene in various solid tumor cell lines (Wang et al., 2015), and silencing of the TPM1 gene confers the glioma U251 cells with radioresistance (Du et al., 2015). As our findings indicate a positive correlation between reduced TPM1 expression and decreased proliferation or increased apoptosis of rNCSCs without alteration of the actin cytoskeleton under hyperoxia, further studies will be required to unravel which downstream effectors of TPM1 link reduced TPM1 expression with the regulatory machinery of cell cycle and apoptosis without affecting stress fiber formation.

It is noteworthy that, under oxidative stress, nuclear-to-cytoplasmic translocation of S100A2 occurred in normal and immortalized but not malignant human keratinocytes, although both immortalized and malignant keratinocytes lacked normal TP53 proteins (Zhang et al., 2002). In this study, we found that incubation with 1 mM of the antioxidant NAC was sufficient to inhibit nuclear-to-cytoplasmic translocation of S100A2 in the rNCSCs cultured at 80% O_2 without affecting cell viability (Figs. (2 and 8)E, 10), in agreement with an oxidative stress-induced translocation of S100A2 (Zhang et al., 2002). It has been proposed that nuclear-to-cytoplasmic translocation of S100A2 in human keratinocytes may result from oxidative stress-induced conformational change of S100A2 proteins (Zhang et al., 2002), which may also be plausible in the rNCSCs cultured at 80% O_2, as we failed to detect altered expression levels of *S100a2* mRNA in rNCSCs under different oxygen tensions. Of interest, previous experiments of knocking down or knocking out the NADPH oxidase 4 (Nox4) have reported that an appropriate level of oxidative stress or ROS is required for proper differentiation and survival of both mouse and rat NCSCs (Lee et al., 2014). It remains to be studied whether S100A2 is a downstream effector of Nox4 or other Nox isozymes in NCSCs in response to hyperoxia, and whether S100A2 plays a role in regulating fate determination and/or differentiation of NCSCs.

Taken together, our study demonstrates for the first time that two extreme oxygen tensions, 0.5% and 80% O_2, differentially regulate NCSC viability and proliferation via two distinct signaling pathways, with hypoxia activating the HIF1α–CXCR4 pathway to enhance proliferation, and hyperoxia up-regulating TP53 and CDKN1A and down-regulating TPM1 to suppress proliferation and induce apoptosis. Understanding the molecular mechanisms underlying the respectively positive and negative effects of hypoxia and hyperoxia on NCSC proliferation is beneficial for finding appropriate ways to increase the regenerative capability and therapeutic potential of adult NCSCs.

Experimental Procedures

Isolation and Culture of rNCSCs

Animals used in this study were purchased from the National Laboratory Animal Center of National Applied Research Laboratories (Taipei, Taiwan), and approval was received from the Institutional Animal Care and Utilization Committee in the Laboratory Animal Center of National Defense Medical Center. The procedures of isolating, culturing and expanding rat NCSCs in vitro have been described previously (Lin et al., 2016). A total of six male and six female Sprague-Dawley rats at 6- to 8-weeks-old were killed by carbon dioxide euthanasia, followed by whole-body immersion in a 1:1 mixture of betadine and hydrogen peroxide for approximately 3 min for disinfection. After squirting the facial region with 75% ethanol, the rats were placed on a dissection microscope in a laminar flow hood and the whisker pads dissected and pooled in HBSS (Hank's balanced salt solution, Thermo Fisher Scientific Co., Waltham, MA). The whisker follicles were then cut with straight scissors without injuring hair bulbs, and loose adipose and dermal tissues were flushed out with HBSS buffer. The clean hair follicles were pinned onto Sylgard-coated glass petri dish and cut longitudinally with a microblade till the appearance of blood, which was then flushed out with HBSS. After making a transverse cut above the level of the cavernous sinus and another cut at the level within the ring sinus, the hair bulges were readily rolled out of the collagen capsule with a bent tungsten needle and subsequently washed in a new culture plate in HBSS.

After washing, the isolated hair follicles were individually cultured in the RPMI 1640 medium supplemented with L-glutamine (Thermo Fisher Scientific Co.), 15% fetal bovine serum (HyClone, Thermo Fisher Scientific), and 4% AmnioMAX^{TM}-II complete medium (Thermo Fisher Scientific Co.) in new 10-cm petri dishes at 37 degC with 5% CO_2 and air balance. The dermal papilla explants of hair follicles will outgrow and adhere to the petri dishes. Half of the old culture medium was replaced with new freshly made medium every day. After 4 to 5 days, it was detected under the microscope that highly migratory cells emigrated out of the dermal papilla explants and showed stellate morphology and absence of cell–cell contacts. These cells are rat neural crest stem cells (rNCSCs). The emigrated rNCSCs were then digested with 0.0.5% trypsin-EDTA (Thermo Fisher Scientific) for 2 min at 37 degC, centrifuged for 5 min at 300 g, and then passaged to be seeded in new petri dishes at a density of 1×10^6/ml. Subsequently, rNCSCs were passaged every 3–4 days to avoid a high cell density stimulating rNCSC differentiation. The rNCSCs after 4−8 passages were used for the following experiments.

Isolation and Culture of rMSCs

rMSCs were isolated from the bone marrow of the tibia and femur of the same Sprague-Dawley rats used to extract rNCSCs, following the procedure described previously (Saini et al., 2013; Lotfy et al., 2014). Briefly, the bone marrow was flushed from the ends of the sterilized and cut tibia and femur using Dulbecco's modified Eagle's medium (DMEM) (Thermo Fisher Scientific) by 27-gauge needles, and subsequently filtered through 70-μm Corning® cell strainers (Sigma-Aldrich, St. Louis, MO).

The bone marrow cells were then cultured in low glucose DMEM/GlutaMAX supplemented with 10% fetal bovine serum (HyClone, Thermo Fisher Scientific), 30 U/ml penicillin, and 30 μg/ml streptomycin (Thermo Fisher Scientific) at 37 degC under 5% CO_2 and 21% O_2. After three passages, the rMSC lineage was confirmed by fluorescence-assisted cell sorting (FACS), which detected positive staining signals with the anti-CD90 antibody (mouse monoclonal with the clone number MRC OX-7; 1:1,000 dilution; Abcam, Cambridge, MA) and negative staining signal with the anti-CD45 antibody (rabbit polyclonal; 1:100 dilution; Abcam). The rMSCs after three passages were used for the following experiments.

Culture of rNCSCs and rMSCs Under Various Oxygen Tensions

rNCSCs after the 4^{th}–8^{th} passages and rMSCs after the 3^{rd} passage were seeded at a density of 6×10^4 cells/ml in several 12-well culture plates (Nunc, Thermo Fisher Scientific) and placed in three separate tri-gas SMA-165DS incubators (ASTEC Co., Ltd., Japan). One of the tri-gas incubators was set up with 5%CO_2/balance air (normoxia), one set up with 1% O_2/5% CO_2/balance N_2 (hypoxia), and another set up with 40% or 80% O_2/5% CO_2/balance N_2 (hyperoxia). Because the smallest value of the oxygen tension setting for the SMA-165DS incubator is 1%, a C-Chamber hypoxia chamber connected to a ProOx P110 controller (BioSpherix Co., Ltd., Parish, NY) was applied in the incubator to achieve a hypoxic environment with 0.5% O_2 inside the chamber. The actual concentration of dissolved oxygen in the cell culture medium was detected by an 8403 D.O. meter (AZ Instrument Corp., Taichung City, Taiwan). According to the manufacturer's instructions, the D.O. meter was calibrated to 21% O_2 in the air-saturated water and to 0% O_2 in the oxygen-free water containing 10 g/L of sodium sulfite and 50 μg/L of cobalt nitrate.

Before culturing under various oxygen tensions, one group of rNCSCs was transfected with either *Cxcr4* or *Hif1α* siRNA to inhibit *Cxcr4* or *Hif1α* expression (as described below). To inhibit CXCR4 signaling, the CXCR4-specific antagonist AMD3100 (Sigma-Aldrich, St. Louis, MO) was added to the final concentration of 10 μM in the medium, as described previously (Kim et al., 2010; Spinello et al., 2011), and rNCSCs were cultured in the AMD3100-containing medium under hypoxia (0.5% O_2) for 36 hr. To inhibit cytoplasmic translocation of S100A2, the antioxidant NAC (Sigma-Aldrich) was added to the final concentration of 1 mM in the medium, as described previously (Lu et al., 2010; Berniakovich et al., 2012), and rNCSCs were cultured in the NAC-containing medium under hyperoxia (40% or 80% O_2) for 36 hr. For decreased or increased oxygen cultures, the culturing plates containing rNCSCs were not placed into each incubator until the respective hypoxia or hyperoxia environment had been set up for at least 24 hr. The 12-well plates containing rNCSCs were cultured separately at 0.5%, 1%, 20%, and 40% and/or 80% oxygen levels for 36 hr and then removed for total cell number counting and immunostaining with various antibodies (as described below).

Cell Counting

Total numbers of rNCSCs were counted by both the hemocytometer and ADAM-MC automatic cell counter by NanoEnTek Inc. (Pleasanton, CA). Both methods obtained identical results. For counting by the hemocytometer, we diluted the culture medium containing rNCSCs for 10-fold and extracted 10 μl of it to mix with an equal volume (10 μl) of trypan blue. As apoptotic and necrotic cells had damaged plasma membranes permeable to trypan blue staining and hence were deep blue-colored, only the semitransparent and round cells were live and counted.

Cell Viability Analyses

The cell viability was analyzed by the Vybrant® MTT (3-(4,5-dimethylthiazol-2-yl)- 2,5-diphenyltetrazolium bromide) cell viability assay kit (Thermo Fisher Scientific). Briefly, 10 μl of 12 mM MTT stock solution was added per 100 μl of freshly replaced medium containing rNCSCs, followed by incubation at 37 degC for 2 hr, and the reaction was terminated by adding 100 μl of the sodium dodecyl sulfate (SDS)-HCl solution and incubating at 37 degC for 4 hr. The relative concentration of the solubilized formazan was then determined by reading the optical absorbance at 570 nm. The viability of rNCSCs cultured at 20% O_2 for 12 hr without any treatment was set up as the control value (i.e., 100% viability).

Normobaric Hypoxia and Hyperoxia Exposure Systems

The Sprague-Dawley rats were divided into three groups and exposed to various oxygen tensions for 36 hr: one group was maintained at $89.0 \pm 0.5\%$ O_2 (for hyperoxic exposure), one group was maintained in room air, i.e., at 21% O_2 (for normoxic exposure), and another group was maintained at $7.0 \pm 0.5\%$ O_2 (for hypoxic exposure). Each group contains a total of six rats, with three male or three female rats placed together in a 33-L Plexiglas glove chamber (Terra Universal, Inc., Fullerton, CA), which was connected to either an N_2 (for hypoxia) or O_2 (for hyperoxia) reservoir cylinder, and had a double-doored entry port that would allow entry and exit of animals without measurably altering the oxygen concentration inside the chamber. The gas outflow rate was controlled by a solenoid valve automatically adjusted by an S-3A oxygen analyzer (AEI Technologies, Inc., Pittsburgh, PA). The CO_2 concentration inside the chambers was maintained at $\leq$0.2% by a baralym scrubber and continuously monitored by a capnograph. The relative humidity inside the chambers was kept at $\leq$70% using anhydrous calcium sulfate. To minimize emission of urinary ammonia, boric acid was also added inside the chambers. All protocols for animal experiments had been approved by the Institutional Animal Care and Utilization Committee in the Laboratory Animal Center of National Defense Medical Center.

Whisker Hair Follicle Tissue Preparation and Analyses of Proliferation, Hypoxia, Oxidative Stress, and Apoptosis

Two hours before the end of the hypoxic or hyperoxic exposure, all Sprague-Dawley rats were injected via the tail vein with 200 μg/g of body weight of 5-bromo-2-deoxyuridine (BrdU) (Sigma-Aldrich), and the hypoxia- and normoxia-exposed rats were also injected with 100 μg/g of body weight of hypoxyprobe-1 (HypoxyprobeTM, Natural Pharmacia Intl. Inc., Belmont, MA). The whisker pads containing hair follicles were harvested from the animals that had exposed to various oxygen tensions for 36 hr, and half of the normoxia- and hyperoxia-exposed whisker pads were incubated in HBSS containing 5 μM of CellROX® Green staining reagent at 37 degC for 1 hr before fixation. All of the whisker pads were then fixed with 4% paraformaldehyde (PFA) (Sigma-Aldrich) in 1 × phosphate buffered saline (PBS) for 12 hr at 4 degC, followed by cryopreservation in sucrose solutions with increasing concentrations and freezing in the Tissue-Tek® O.C.T. compound (Sakura Finetek Co., Ltd., Japan).

Cryostat sections were cut at 10-μm thickness, and half of the hypoxia- or normoxia-exposed tissue sections were then double immunostained with the anti-SOX10 antibody (rabbit polyclonal; 1:1,000 dilution; Abcam) and anti-hypoxyprobe-1 antibody (mouse monoclonal; 1:200 dilution; Natural Pharmacia Intl. Inc.), while half of the hyperoxia-exposed tissue sections were double stained with the CellROX® Green oxidative stress reagent (Thermo Fisher Scientific) and the anti-SOX10 antibody. The other half of hair follicle tissue sections in all groups were double stained with the anti-BrdU antibody (mouse monoclonal; 1:500 dilution; Sigma-Aldrich) and the Click-iT® TUNEL Alexa Fluor® 488 Imaging Kit (Thermo Fisher Scientific). The Vectashield Antifade Mounting Medium (Vector Laboratories, Burlingame, CA) was applied to mount coverslips onto the immunostained tissue sections.

siRNA Transfection

The oligonucleotides of *Cxcr4* siRNA, *Hif1α* siRNA, *Tp53* siRNA, *S100a2* siRNA, negative control siRNA and positive control (*Tbp*: TATA box-binding protein) siRNA were all obtained from Thermo Fisher Scientific Co., Waltham, MA. The sequence of the 22-mer antisense *Cxcr4* siRNA was 5′-CUGUCAUGCUCCUCAGCUUCd TdT-3′, corresponding to nucleotides 267–286 of the NCBI reference sequence NM_022205. The sequence of the 22-mer antisense *Hif1α* siRNA was 5′-GUGAGCCUCAUAACAGAAGCdTdT-3′, corresponding to nucleotides 195–214 of the NCBI reference sequence NM_024359. The sequence of the 22-mer antisense *Tp53* siRNA was 5′-GAGGAAGAAGUUUCCAUAAGdTdT-3′, corresponding to nucleotides 86–105 of the NCBI reference sequence X13058. The sequence of the 22-mer antisense *S100a2* siRNA was 5′-CAUCUGACUUAAAUUGAAGGdTdT-3′, corresponding to nucleotides 572–591 of the NCBI gene ID LOC100910139.

We used the *Silencer® Tbp* siRNA (Thermo Fisher Scientific) for rat as a positive control and the *Silencer®* Negative Control siRNA (Thermo Fisher Scientific) as a negative control. Among the house keeping genes, the *Tbp* instead of *Gapdh* siRNA was chosen as a positive control because previous studies have demonstrated that *Gapdh* gene expression is subject to regulation by hypoxia (Zhong and Simons, 1999; Yamaji et al., 2003; Foldager et al., 2009; Higashimura et al., 2011), whereas *Tbp* expression is relatively unaffected by changes of oxygen tensions (Foldager et al., 2009; Caradec et al., 2010). 3×10^5 cells/ml of rNCSCs seeded in six-well culture plates (Nunc, Thermo Scientific Co., Waltham, MA) were grown to be 70–90% confluent, washed and transferred to serum-free medium, followed by transfection with 2.5 μg of siRNA per well using the Lipofectamine® 2000 Reagent kit (Invitrogen, Thermo Fisher Scientific) in accordance with the manufacturer's instructions. After 24 hr, the siRNA-transfected rNCSCs were washed and transferred to complete maintenance medium, and then cultured at 0.5% O_2 at a density of 6×10^4 cells/ml in 12-well plates.

Transfection With CMV-containing Expression Vectors

Both of the empty *pCMV6-Kan/Neo* Rat TrueClone and *pCMV6-Tp53* Rat cDNA TrueClone vectors were obtained from OriGene Technologies, Inc. (Rockville, MD). A total of 3×10^5 cells/ml of rNCSCs seeded in 6-well culture plates (Nunc, Thermo Scientific Co., Waltham, MA) were grown to be 70–90% confluent, washed and transferred to serum-free medium, followed by transfection with 3 μg of siRNA per well using the Lipofectamine® 2000 Reagent kit (Invitrogen, Thermo Fisher Scientific) in accordance with the manufacturer's instructions. After 24 hr, the siRNA-transfected rNCSCs were washed and transferred to complete maintenance medium, and then cultured at 0.5% O_2 at a density of 6×10^4 cells/ml in 12-well plates.

Immunofluorescence Staining

After culturing at 0.5%, 20%, 40%, or 80% oxygen levels for 36 hr, the culture medium in the 12-well plates containing rNCSCs was aspirated carefully without touching the cells, which were adhered to the bottom of the plates. rNCSCs were then washed three times in 1 × PBS at pH 7.4, for 5 min each time, followed by fixation in 1 ml of 4% PFA (Sigma-Aldrich) in PBS for 20 min. After washing with 1 × PBS three times again, the fixed cells were permeabilized with 0.5% Triton X-100 for 10 min, then blocked with 10% bovine serum albumin (BSA, Sigma-Aldrich) in 1 × PBS for 1 hr, to prevent high background signals of immunostaining from nonspecific binding of primary and secondary antibodies.

Following blocking, rNCSCs were incubated with the following primary antibodies or conjugates diluted in 1 × PBS at 4 degC overnight: anti-CDKN1A ($p21^{CIP1/WAF1}$) (mouse monoclonal with the clone number F-5; 1:100 dilution; Sigma-Aldrich), anti-cortactin (rabbit monoclonal; 1:250 dilution; Abcam), anti-CXCR4 (rabbit polyclonal; 1:100 dilution; Abcam), anti-FOXD3 (rabbit polyclonal; 1:100 dilution; Santa Cruz Biotechnology), anti-HIF1α (mouse monoclonal with the clone number H1alpha 67; 1:100 dilution; Santa Cruz Biotechnology), anti-NGFR (rabbit polyclonal; 1:400 dilution; Abcam), anti-S100A2 (mouse monoclonal with the clone number SH-L1; 1:1,000 dilution; Thermo Fisher Scientific), anti-SNAIL (mouse monoclonal with the clone number G-7; 1:100 dilution; Santa Cruz Biotechnology), anti-SOX10 (rabbit polyclonal; 1:1,000 dilution; Abcam), anti-TP53 (rabbit polyclonal; 1:200 dilution; Abcam), anti-TPM1 (rabbit polyclonal; 1:250 dilution; Abcam), bovine pancreatic deoxyribonuclease I conjugated to Alexa Fluor® 594 (1:100 dilution; Thermo Fisher Scientific), and phalloidin conjugated to Alexa Fluor® 488 (1:40 dilution; Thermo Fisher Scientific). For isotype

negative controls, mouse monoclonal IgG1 (with the clone number NCG01) and rabbit polyclonal IgG from Abcam were applied at the same concentration as the respective primary antibodies.

On the second day, the cells were washed three times in 1 × PBS and blocked for 20 min with 10% BSA in 1 × PBS, followed by incubation at room temperature for 1 hr with the following secondary antibodies conjugated with fluorophores: donkey anti-mouse Alexa Fluor® 488, donkey anti-mouse Alexa Fluor® 555, donkey anti-rabbit Alexa Fluor® 488, and donkey anti-rabbit Alexa Fluor® 555 (Molecular Probes, Thermo Fisher Scientific). After 1 hr, the cells were washed in 1 × PBS again, followed by counter-staining with 10 μg/ml of DAPI (1:1,000 dilution; Molecular Probes, Thermo Fisher Scientific) in 1 × PBS for 10 min. Subsequently, the cells were washed and stored in 1 × PBS, followed by photographing under the AXIO observer inverted fluorescence microscope (Zeiss). In line with the fluorescence intensities of different fluorochromes, the exposure time of the AxioCam HRc color CCD camera was set as 350 msec for DAPI, 400 msec for Alexa Fluor® 488, and 450 msec for Alexa Fluor® 555. Both isotype-negative controls and no-primary-antibody controls showed no specific staining with only very few background signals (data not shown).

For analysis of cell proliferation, the Click-iT™ EdU Alexa Fluor® 555 Imaging Kit (Thermo Fisher Scientific) was used. Briefly, 6×10^4 cells/ml of rNCSCs were cultured in the 1:1 volume-to-volume mixture of the maintenance medium and 20 μM solution of EdU for 12 hr in 12-well plates, followed by fixation in 4% PFA and permeabilization with 0.5% Triton X-100, same as described above in the immunostaining procedure. After washing with 1 × PBS containing 3% BSA, 0.5 ml of Click-iT™ reaction cocktail was added to each well and incubated for 30 min with protection from light. After EdU labeling, the rNCSCs were washed three times in 1 × PBS and blocked for 20 min with 10% BSA in 1 × PBS, and then immunostained with primary antibodies.

For analysis of cell apoptosis, the Click-iT® TUNEL Alexa Fluor® 488 Imaging Kit (Thermo Fisher Scientific) was used. Briefly, rNCSCs cultured in 12-well plates were fixed and permeabilized as described above in the immunostaining procedure, followed by washing with deionized and distilled water twice and incubation with TdT reaction buffer for 10 min at room temperature. After removing the TdT reaction buffer, the TdT reaction cocktail was added to each well and incubated for 1 hr at 37 degC, followed by washing twice with 1 × PBS containing 3% BSA. The rNCSCs were then incubated with the Click-iT® reaction cocktail for 30 min at room temperature with protection from light, washed in 1 × PBS three times and blocked with 10% BSA in 1 × PBS for 20 min, and then immunostained with primary antibodies.

Quantitative Analyses of Immunostaining

The image files obtained from Zeiss fluorescence microscope were input into the Count Nuclei/Cell Sorting Application Module for MetaMorph (MetaMorph Offline vers. 7.0; Universal Imaging Corporation™, Buckinghamshire, UK) for quantitative analyses and comparison among different groups of rNCSCs in vitro and among different tissue sections of rat whisker hair follicles in vivo. Briefly, for cell counting, the numbers of rNCSC or hair follicle cells/nuclei stained with different colors of fluorescence (red or green) and the total numbers of DAPI-stained nuclei were, respectively, counted on the image files of each experimental group. The average percentages of positive rNCSC or hair follicle cells/nuclei in each experimental group were calculated as: (the summary of numbers of cells or nuclei stained with red or green fluorescence on all images)/(the summary of total numbers of $DAPI^+$ nuclei on all images) × 100%.

For comparison of fluorescent intensities, a specified unit of area (e.g., a defined range of the cytoplasm or nucleus) in the untreated rNCSCs cultured at 20% O_2 was set up to quantify the fluorescent intensity within the area, which was recorded as a standard value. The same unit of area was picked up from rNCSCs in the other experimental groups (i.e., cultured under hypoxia or hyperoxia, and/or siRNA-transfected or AMD3100- or NAC-incubated), followed by quantification of fluorescent intensity within the area and comparison with the standard value. The relative intensity of a specific marker within an experimental group was calculated by the summation of relative values obtained from all units of areas on all image files within that group, and was quantified as a fold-change of the standard value.

Western Blot Analyses of Cytoplasmic and Nuclear Protein Extracts

The cytoplasmic and nuclear protein fractions of rNCSCs were sequentially extracted using the NE-PER™ Nuclear and Cytoplasmic Extraction Reagents (Thermo Fisher Scientific Co.) according to the manufacturer's instructions. Briefly, 1×10^6 rNCSCs were trypsinized and centrifuged in a 1.5-ml microcentrifuge tube, lysed with the ice-cold CER I and CER II reagents sequentially, followed by the second centrifugation to obtain supernatants containing the cytoplasmic extracts. The pellet deposition after the second centrifugation was further lysed by the ice-cold NER reagent and centrifuged again to obtain supernatants containing the nuclear extracts.

Equal amounts of cytoplasmic or nuclear protein extracts from each group of rNCSCs were separated using SDS-10% polyacrylamide gel electrophoresis and transblotted onto polyvinylidene difluoride (PVDF) membranes (Millipore, Bedford, MA). Protein concentration was quantified using the Pierce™ BCA Protein Assay Kit (Thermo Fisher Scientific). Immunoblotting was performed with the same primary antibodies applied for immunofluorescence staining (described above). β-Actin and TBP served, respectively, as the cytoplasmic and nuclear extract markers and loading controls, and were immunoblotted with the anti-β-actin (rabbit polyclonal; 1:100 dilution; Santa Cruz Biotechnology) and anti-TBP (mouse monoclonal with the clone number mAbcam 51841; 1:1,000 dilution; Abcam) antibodies. Glyceraldehyde 3-phosphate dehydrogenase is not an appropriate loading control for our study, as its gene expression has been reported to be subject to regulation by hypoxia (Zhong and Simons, 1999; Yamaji et al., 2003; Foldager et al., 2009; Higashimura et al., 2011). For negative controls, the PVDF membranes carrying the cytoplasmic or nuclear protein extracts from different groups of rNCSCs were immunoblotted with either mouse monoclonal IgG1 or rabbit polyclonal IgG from Abcam. The signals of immunoblots were visualized with the Amersham ECL Western Blotting Detection Kit (GE Healthcare Life Sciences, Chicago, IL) followed by exposure to X-ray films.

Real-time Quantitative RT-PCR

Immediately after culturing for 36 hr under various oxygen tensions, total RNA was extracted from the untreated, NAC-

incubated, and siRNA or *CMV* vector transfected rNCSCs using the RNAqueous®-Micro total RNA isolation kit (Ambion, Thermo Fisher Scientific) followed by reverse transcription with SuperScript® III First-Strand Synthesis System (Invitrogen, Thermo Fisher Scientific). The primer sequences for each different cDNA for analyses are: forward primer 5′-GCTGGTTGAGGAGGAGTT-3′ and reverse primer 5′-CATCTTTTTGGGCTCGGCTT-3′ for *Tpm1*, forward primer 5′-ACCGTGAATCTTGGCTGTAAAC-3′ and reverse primer 5′-CGCAGTTGTTCGTGGCTCTC-3′ for *Tbp*, forward primer 5′-CATGGATACGTGAGGGGTGC-3′ and reverse primer 5′-CCTC GTGACTTTCCTGTCTCA-3′ for *S100a2*, and forward primer 5′-CATCGAGCTCCCTCTGAGTC-3′ and reverse primer 5′-CTGTGG TGGGCAGAATATCA-3′ for *Tp53*.

The total cDNA templates synthesized from the extracted total mRNA were then mixed with the aforementioned multiplex primer sets and the Platinum® SYBR® Green qPCR SuperMix-UDG (Invitrogen, Thermo Fisher Scientific), followed by real-time quantitative PCR reactions using the Applied Biosystems® 7500 Fast Real-time PCR System (Applied Biosystems Group, Thermo Fisher Scientific) located in the Instrument Center of National Defense Medical Center. Because it has been demonstrated that 18S rRNA and *β-Actin* are the two least stable reference genes for quantitative PCR studies in rat carotid bodies under hyperoxia and/or hypoxia conditions (Kim et al., 2011), we selected *Tbp* mRNA, which was shown to be one of the best reference gene under various oxygen tensions (Kim et al., 2011), as a normalization control for the mRNA expression analyses in this study. The cycling program was set up as 2 min hold at 50 degC for UDG incubation followed by 5 min of denaturation at 95 degC and 50 cycles of denaturation at 95 degC for 15 sec, annealing at 60 degC for 45 sec, and elongation at 95 degC for 1 min. The expected sizes of the RT-PCR products for *Tpm1, Tbp, S100a2*, and *Tp53* mRNA are, respectively, 134, 123, 108, and 80 base pairs. The results of real-time PCR were analyzed by the DDCt method based on the cycle threshold (Ct) values. The mean Ct values for *Tpm1, S100a2*, and *Tp53* mRNA were normalized against the mean Ct values for *TBP* mRNA from the same samples, and the quantitative expression of each mRNA was calculated using $2^{-\Delta\Delta Ct}$, where $\Delta\Delta Ct = \Delta Ct^{mRNA} - \Delta Ct^{Tbp\ mRNA}$. The relative levels of *Tpm1, S100a2*, and *Tp53* expression in different samples were calculated in comparison with the level of *TBP* expression in the rNCSCs cultured at 20% O_2, which was presumptively set up as 1.0.

Statistical Analyses

For statistical analyses, we performed one-way ANOVA with post-hoc tests of Duncan's multiple range test and Scheffé's method, which analyzed both the within-group variation and between-group variation and calculated the relative ratios by use of the SPSS 20.2 software (International Business Machines Corporation). The data of total cell numbers after 36-hr culture, positive cell percentages for different markers, and relative expression levels of various cytoplasmic and nuclear proteins were all analyzed and compared within and between distinct groups of rNCSCs ($n = 12$ in each group) by one-way ANOVA.

Acknowledgments

We acknowledge technical services provided by the Instrument Center of National Defense Medical Center. Yi-Hui Chen was supported by grants from the Medical Affairs Bureau–Ministry of National Defense, R.O.C. Author Disclosure Statement: No competing financial interests exist.

References

Abdollahi H, Harris LJ, Zhang P, McIlhenny S, Srinivas V, Tulenko T, DiMuzio PJ. 2011. The role of hypoxia in stem cell differentiation and therapeutics. J Surg Res 165:112–117.

Adams MS, Bronner-Fraser M. 2009. Review: the role of neural crest cells in the endocrine system. Endocr Pathol 20:92–100.

Alcaraz-Garcia MJ, Albaladejo MD, Acevedo C, Olea A, Zamora S, Martinez P, Parra S. 2008. Effects of hyperoxia on biomarkers of oxidative stress in closed-circuit oxygen military divers. J Physiol Biochem 64:135–141.

Atashi F, Modarressi A, Pepper MS. 2015. The role of reactive oxygen species in mesenchymal stem cell adipogenic and osteogenic differentiation: a review. Stem Cells Dev 24:1150–1163.

Aybar MJ, Nieto MA, Mayor R. 2003. Snail precedes slug in the genetic cascade required for the specification and migration of the Xenopus neural crest. Development 130:483–494.

Baek WY, Kim YJ, de Crombrugghe B, Kim JE. 2013. Osterix is required for cranial neural crest-derived craniofacial bone formation. Biochem Biophys Res Commun 432:188–192.

Barriga EH, Maxwell PH, Reyes AE, Mayor R. 2013. The hypoxia factor Hif-1alpha controls neural crest chemotaxis and epithelial to mesenchymal transition. J Cell Biol 201:759–776.

Belmadani A, Jung H, Ren D, Miller RJ. 2009. The chemokine SDF-1/CXCL12 regulates the migration of melanocyte progenitors in mouse hair follicles. Differentiation 77:395–411.

Berniakovich I, Laricchia-Robbio L, Izpisua Belmonte JC. 2012. N-acetylcysteine protects induced pluripotent stem cells from in vitro stress: impact on differentiation outcome. Int J Dev Biol 56: 729–735.

Bigarella CL, Liang R, Ghaffari S. 2014. Stem cells and the impact of ROS signaling. Development 141:4206–4218.

Bitterman H. 2010. Therapeutic effects of hyperoxic ventilation during shock. Transfusion Altern Transfus Med 11:156–163.

Canton M, Skyschally A, Menabo R, Boengler K, Gres P, Schulz R, Haude M, Erbel R, Di Lisa F, Heusch G. 2006. Oxidative modification of tropomyosin and myocardial dysfunction following coronary microembolization. Eur Heart J 27:875–881.

Caradec J, Sirab N, Keumeugni C, Moutereau S, Chimingqi M, Matar C, Revaud D, Bah M, Manivet P, Conti M, Loric S. 2010. 'Desperate house genes': the dramatic example of hypoxia. Br J Cancer 102:1037–1043.

Carmeliet P, Dor Y, Herbert JM, Fukumura D, Brusselmans K, Dewerchin M, Neeman M, Bono F, Abramovitch R, Maxwell P, Koch CJ, Ratcliffe P, Moons L, Jain RK, Collen D, Keshert E. 1998. Role of HIF-1alpha in hypoxia-mediated apoptosis, cell proliferation and tumour angiogenesis. Nature 394:485–490.

Chen S, Zhang M, Xing L, Wang Y, Xiao Y, Wu Y. 2015. HIF-1alpha contributes to proliferation and invasiveness of neuroblastoma cells via SHH signaling. PLoS One 10:e0121115.

Chew YC, Adhikary G, Wilson GM, Reece EA, Eckert RL. 2011. Protein kinase C (PKC) delta suppresses keratinocyte proliferation by increasing p21(Cip1) level by a KLF4 transcription factor-dependent mechanism. J Biol Chem 286:28772–28782.

Chipuk JE, Kuwana T, Bouchier-Hayes L, Droin NM, Newmeyer DD, Schuler M, Green DR. 2004. Direct activation of Bax by p53 mediates mitochondrial membrane permeabilization and apoptosis. Science 303:1010–1014.

Cichorek M, Wachulska M, Stasiewicz A, Tyminska A. 2013. Skin melanocytes: biology and development. Postepy Dermatol Alergol 30:30–41.

Clewes O, Narytnyk A, Gillinder KR, Loughney AD, Murdoch AP, Sieber-Blum M. 2011. Human epidermal neural crest stem cells (hEPI-NCSC)-characterization and directed differentiation into osteocytes and melanocytes. Stem Cell Rev 7:799–814.

Coura GS, Garcez RC, de Aguiar CB, Alvarez-Silva M, Magini RS, Trentin AG. 2008. Human periodontal ligament: a niche of neural crest stem cells. J Periodontal Res 43:531–536.

Csete M, Walikonis J, Slawny N, Wei Y, Korsnes S, Doyle JC, Wold B. 2001. Oxygen-mediated regulation of skeletal muscle satellite

cell proliferation and adipogenesis in culture. J Cell Physiol 189: 189–196.
d'Aquino R, Tirino V, Desiderio V, Studer M, Angelis GCD, Laino L, Rosa AD, Nucci DD, Martino S, Paino F, Sampaolesi M, Papaccio G. 2011. Human neural crest-derived postnatal cells exhibit remarkable embryonic attributes either in vitro or in vivo. Eur Cell Mater 21:304–316.
Dai J, Kuang Y, Fang B, Gong H, Lu S, Mou Z, Sun H, Dong Y, Lu J, Zhang W, Zhang J, Wang Z, Wang X, Shen G. 2013a. The effect of overexpression of Dlx2 on the migration, proliferation and osteogenic differentiation of cranial neural crest stem cells. Biomaterials 34:1898–1910.
Dai JW, Yuan H, Shen SY, Lu JT, Zhu XF, Yang T, Zhang JF, Shen GF. 2013b. p75 neurotrophin receptor positive dental pulp stem cells: new hope for patients with neurodegenerative disease and neural injury. Shanghai Kou Qiang Yi Xue 22:469–472.
Darekar S, Georgiou K, Yurchenko M, Yenamandra SP, Chachami G, Simos G, Klein G, Kashuba E. 2012. Epstein-Barr virus immortalization of human B-cells leads to stabilization of hypoxia-induced factor 1 alpha, congruent with the Warburg effect. PLoS One 7:e42072.
Deb S, Johansson I, Byrne D, Nilsson C, Investigators k, Constable L, Fjallskog ML, Dobrovic A, Hedenfalk I, Fox SB. 2014. Nuclear HIF1A expression is strongly prognostic in sporadic but not familial male breast cancer. Mod Pathol 27:1223–1230.
del Barrio MG, Nieto MA. 2002. Overexpression of Snail family members highlights their ability to promote chick neural crest formation. Development 129:1583–1593.
do Carmo A, Patricio I, Cruz MT, Carvalheiro H, Oliveira CR, Lopes MC. 2010. CXCL12/CXCR4 promotes motility and proliferation of glioma cells. Cancer Biol Ther 9:56–65.
Don-Salu-Hewage AS, Chan SY, McAndrews KM, Chetram MA, Dawson MR, Bethea DA, Hinton CV. 2013. Cysteine (C)-x-C receptor 4 undergoes transportin 1-dependent nuclear localization and remains functional at the nucleus of metastatic prostate cancer cells. PLoS One 8:e57194.
Du HQ, Wang Y, Jiang Y, Wang CH, Zhou T, Liu HY, Xiao H. 2015. Silencing of the TPM1 gene induces radioresistance of glioma U251 cells. Oncol Rep 33:2807–2814.
El-Helou V, Beguin PC, Assimakopoulos J, Clement R, Gosselin H, Brugada R, Aumont A, Biernaskie J, Villeneuve L, Leung TK, Fernandes KJ, Calderone A. 2008. The rat heart contains a neural stem cell population; role in sympathetic sprouting and angiogenesis. J Mol Cell Cardiol 45:694–702.
Escot S, Blavet C, Hartle S, Duband JL, Fournier-Thibault C. 2013. Misregulation of SDF1-CXCR4 signaling impairs early cardiac neural crest cell migration leading to conotruncal defects. Circ Res 113:505–516.
Fernandes TG, Diogo MM, Fernandes-Platzgummer A, da Silva CL, Cabral JM. 2010. Different stages of pluripotency determine distinct patterns of proliferation, metabolism, and lineage commitment of embryonic stem cells under hypoxia. Stem Cell Res 5:76–89.
Foldager CB, Munir S, Ulrik-Vinther M, Soballe K, Bunger C, Lind M. 2009. Validation of suitable house keeping genes for hypoxia-cultured human chondrocytes. BMC Mol Biol 10:94.
Forristal CE, Wright KL, Hanley NA, Oreffo RO, Houghton FD. 2010. Hypoxia inducible factors regulate pluripotency and proliferation in human embryonic stem cells cultured at reduced oxygen tensions. Reproduction 139:85–97.
Gimona M, Lando Z, Dolginov Y, Vandekerckhove J, Kobayashi R, Sobieszek A, Helfman DM. 1997. Ca2+-dependent interaction of S100A2 with muscle and nonmuscle tropomyosins. J Cell Sci 110(pt 5):611–621.
Goda N, Dozier SJ, Johnson RS. 2003. HIF-1 in cell cycle regulation, apoptosis, and tumor progression. Antioxid Redox Signal 5: 467–473.
Grayson WL, Zhao F, Bunnell B, Ma T. 2007. Hypoxia enhances proliferation and tissue formation of human mesenchymal stem cells. Biochem Biophys Res Commun 358:948–953.
Gronthos S, Brahim J, Li W, Fisher LW, Cherman N, Boyde A, DenBesten P, Robey PG, Shi S. 2002. Stem cell properties of human dental pulp stem cells. J Dent Res 81:531–535.
Guan G, Zhang Y, Lu Y, Liu L, Shi D, Wen Y, Yang L, Ma Q, Liu T, Zhu X, Qiu X, Zhou Y. 2015. The HIF-1alpha/CXCR4 pathway supports hypoxia-induced metastasis of human osteosarcoma cells. Cancer Lett 357:254–264.
Guimaraes-Camboa N, Stowe J, Aneas I, Sakabe N, Cattaneo P, Henderson L, Kilberg MS, Johnson RS, Chen J, McCulloch AD, Nobrega MA, Evans SM, Zambon AC. 2015. HIF1alpha represses cell stress pathways to allow proliferation of hypoxic fetal cardiomyocytes. Dev Cell 33:507–521.
Guo M, Cai C, Zhao G, Qiu X, Zhao H, Ma Q, Tian L, Li X, Hu Y, Liao B, Ma B, Fan Q. 2014. Hypoxia promotes migration and induces CXCR4 expression via HIF-1alpha activation in human osteosarcoma. PLoS One 9:e90518.
Hakim F, Kaitsuka T, Raeed JM, Wei FY, Shiraki N, Akagi T, Yokota T, Kume S, Tomizawa K. 2014. High oxygen condition facilitates the differentiation of mouse and human pluripotent stem cells into pancreatic progenitors and insulin-producing cells. J Biol Chem 289:9623–9638.
Heckmann D, Maier P, Laufs S, Wenz F, Zeller WJ, Fruehauf S, Allgayer H. 2013. CXCR4 expression and treatment with SDF-1alpha or plerixafor modulate proliferation and chemosensitivity of colon cancer cells. Transl Oncol 6:124–132.
Hellewell SC, Yan EB, Agyapomaa DA, Bye N, Morganti-Kossmann MC. 2010. Post-traumatic hypoxia exacerbates brain tissue damage: analysis of axonal injury and glial responses. J Neurotrauma 27:1997–2010.
Higashimura Y, Nakajima Y, Yamaji R, Harada N, Shibasaki F, Nakano Y, Inui H. 2011. Up-regulation of glyceraldehyde-3-phosphate dehydrogenase gene expression by HIF-1 activity depending on Sp1 in hypoxic breast cancer cells. Arch Biochem Biophys 509:1–8.
Hochgreb-Hagele T, Bronner ME. 2013. A novel FoxD3 gene trap line reveals neural crest precursor movement and a role for FoxD3 in their specification. Dev Biol 374:1–11.
Holzwarth C, Vaegler M, Gieseke F, Pfister SM, Handgretinger R, Kerst G, Muller I. 2010. Low physiologic oxygen tensions reduce proliferation and differentiation of human multipotent mesenchymal stromal cells. BMC Cell Biol 11:11.
Horowitz S. 1999. Pathways to cell death in hyperoxia. Chest 116: 64S–67S.
Houle F, Poirier A, Dumaresq J, Huot J. 2007. DAP kinase mediates the phosphorylation of tropomyosin-1 downstream of the ERK pathway, which regulates the formation of stress fibers in response to oxidative stress. J Cell Sci 120:3666–3677.
Houle F, Rousseau S, Morrice N, Luc M, Mongrain S, Turner CE, Tanaka S, Moreau P, Huot J. 2003. Extracellular signal-regulated kinase mediates phosphorylation of tropomyosin-1 to promote cytoskeleton remodeling in response to oxidative stress: impact on membrane blebbing. Mol Biol Cell 14:1418–1432.
Hu D-Y, Li Q, Li B, Dai R-J, Geng L-N, Deng Y-L. 2009. Normobaric hypoxia-induced brain damage in wistar rat. J. Biomed Sci Eng 2:632–636.
Hung SP, Ho JH, Shih YR, Lo T, Lee OK. 2012. Hypoxia promotes proliferation and osteogenic differentiation potentials of human mesenchymal stem cells. J Orthop Res 30:260–266.
Isern J, Garcia-Garcia A, Martin AM, Arranz L, Martin-Perez D, Torroja C, Sanchez-Cabo F, Mendez-Ferrer S. 2014. The neural crest is a source of mesenchymal stem cells with specialized hematopoietic stem cell niche function. eLife 3:e03696.
Ishikawa T, Nakashiro K, Klosek SK, Goda H, Hara S, Uchida D, Hamakawa H. 2009. Hypoxia enhances CXCR4 expression by activating HIF-1 in oral squamous cell carcinoma. Oncol Rep 21: 707–712.
Jacob C, Lotscher P, Engler S, Baggiolini A, Varum Tavares S, Brugger V, John N, Buchmann-Moller S, Snider PL, Conway SJ, Yamaguchi T, Matthias P, Sommer L, Mantei N, Suter U. 2014. HDAC1 and HDAC2 control the specification of neural crest cells into peripheral glia. J Neurosci 34:6112–6122.
Kahn J, Byk T, Jansson-Sjostrand L, Petit I, Shivtiel S, Nagler A, Hardan I, Deutsch V, Gazit Z, Gazit D, Karlsson S, Lapidot T. 2004. Overexpression of CXCR4 on human CD34+progenitors increases their proliferation, migration, and NOD/SCID repopulation. Blood 103:2942–2949.
Kaindl AM, Sifringer M, Zabel C, Nebrich G, Wacker MA, Felderhoff-Mueser U, Endesfelder S, von der Hagen M, Stefovska V, Klose J, Ikonomidou C. 2006. Acute and long-term

proteome changes induced by oxidative stress in the developing brain. Cell Death Differ 13:1097–1109.
Kakudo N, Morimoto N, Ogawa T, Taketani S, Kusumoto K. 2015. Hypoxia enhances proliferation of human adipose-derived stem cells via HIF-1a activation. PLoS One 10:e0139890.
Kayali AG, Lopez AD, Hao E, Hinton A, Hayek A, King CC. 2012. The SDF-1alpha/CXCR4 axis is required for proliferation and maturation of human fetal pancreatic endocrine progenitor cells. PLoS One 7:e38721.
Kelsh RN. 2006. Sorting out Sox10 functions in neural crest development. Bioessays 28:788–798.
Kerosuo L, Nie S, Bajpai R, Bronner ME. 2015. Crestospheres: long-term maintenance of multipotent, premigratory neural crest stem cells. Stem Cell Reports 5:499–507.
Kim HY, Hwang JY, Kim SW, Lee HJ, Yun HJ, Kim S, Jo DY. 2010. The CXCR4 antagonist AMD3100 has dual effects on survival and proliferation of myeloma cells in vitro. Cancer Res Treat 42: 225–234.
Kim I, Yang D, Tang X, Carroll JL. 2011. Reference gene validation for qPCR in rat carotid body during postnatal development. BMC Res Notes 4:440.
Kim J, Lo L, Dormand E, Anderson DJ. 2003. SOX10 maintains multipotency and inhibits neuronal differentiation of neural crest stem cells. Neuron 38:17–31.
Kokovay E, Temple S. 2007. Taking neural crest stem cells to new heights. Cell 131:234–236.
Konig N, Trolle C, Kapuralin K, Adameyko I, Mitrecic D, Aldskogius H, Shortland PJ, Kozlova EN. 2014. Murine neural crest stem cells and embryonic stem cell-derived neuron precursors survive and differentiate after transplantation in a model of dorsal root avulsion. J Tissue Eng Regen Med [epub ahead of print].
Kos R, Reedy MV, Johnson RL, Erickson CA. 2001. The winged-helix transcription factor FoxD3 is important for establishing the neural crest lineage and repressing melanogenesis in avian embryos. Development 128:1467–1479.
Kruger GM, Mosher JT, Bixby S, Joseph N, Iwashita T, Morrison SJ. 2002. Neural crest stem cells persist in the adult gut but undergo changes in self-renewal, neuronal subtype potential, and factor responsiveness. Neuron 35:657–669.
Kunisada T, Tezulka K, Aoki H, Motohashi T. 2014. The stemness of neural crest cells and their derivatives. Birth Defects Res C Embryo Today 102:251–262.
La Noce M, Mele L, Tirino V, Paino F, De Rosa A, Naddeo P, Papagerakis P, Papaccio G, Desiderio V. 2014. Neural crest stem cell population in craniomaxillofacial development and tissue repair. Eur Cell Mater 28:348–357.
LaBonne C, Bronner-Fraser M. 2000. Snail-related transcriptional repressors are required in Xenopus for both the induction of the neural crest and its subsequent migration. Dev Biol 221:195–205.
Le Moan N, Houslay DM, Christian F, Houslay MD, Akassoglou K. 2011. Oxygen-dependent cleavage of the p75 neurotrophin receptor triggers stabilization of HIF-1alpha. Mol Cell 44:476–490.
Lee G, Kim H, Elkabetz Y, Al Shamy G, Panagiotakos G, Barberi T, Tabar V, Studer L. 2007. Isolation and directed differentiation of neural crest stem cells derived from human embryonic stem cells. Nat Biotechnol 25:1468–1475.
Lee JE, Cho KE, Lee KE, Kim J, Bae YS. 2014. Nox4-mediated cell signaling regulates differentiation and survival of neural crest stem cells. Mol Cells 37:907–911.
Lee SH, Lee MY, Han HJ. 2008a. Short-period hypoxia increases mouse embryonic stem cell proliferation through cooperation of arachidonic acid and PI3K/Akt signalling pathways. Cell Prolif 41:230–247.
Lee Y, Kim JM, Lee EJ. 2008b. Functional expression of CXCR4 in somatotrophs: CXCL12 activates GH gene, GH production and secretion, and cellular proliferation. J Endocrinol 199:191–199.
Li HY, Say EH, Zhou XF. 2007. Isolation and characterization of neural crest progenitors from adult dorsal root ganglia. Stem Cells 25:2053–2065.
Li X, Zhang Y. 2010. Effect of Hif1α on proliferation and differentiation of MSC under hypoxia condition in vitro. Heart 96:A56.
Lin SC, Gou GH, Hsia CW, Ho CW, Huang KL, Wu YF, Lee SY, Chen YH. 2016. Simulated microgravity disrupts cytoskeleton organization and increases apoptosis of rat neural crest stem cells via up-regulating CXCR4 expression and RhoA-ROCK1-p38 MAPK-p53 signaling. Stem Cells Dev 25:1172–1193.
Lin YH, Huang YH, Wu MH, Wu SM, Chi HC, Liao CJ, Chen CY, Tseng YH, Tsai CY, Tsai MM, Lin KH. 2013. Thyroid hormone suppresses cell proliferation through endoglin-mediated promotion of p21 stability. Oncogene 32:3904–3914.
Liu H, Liu Y, Liu W, Zhang W, Xu J. 2015. EZH2-mediated loss of miR-622 determines CXCR4 activation in hepatocellular carcinoma. Nat Commun 6:8494.
Liu J, Yang X, Shi W. 2013. Overexpression of CXCR4 in tracheal epithelial cells promotes their proliferation and migration to a stromal cell-derived factor-1 gradient. Exp Biol Med (Maywood) 238:144–150.
Liu MT, Kuan YH, Wang J, Hen R, Gershon MD. 2009. 5-HT4 receptor-mediated neuroprotection and neurogenesis in the enteric nervous system of adult mice. J Neurosci 29:9683–9699.
Liu YL, Yu JM, Song XR, Wang XW, Xing LG, Gao BB. 2006. Regulation of the chemokine receptor CXCR4 and metastasis by hypoxia-inducible factor in non small cell lung cancer cell lines. Cancer Biol Ther 5:1320–1326.
Lokmic Z, Darby IA, Thompson EW, Mitchell GM. 2006. Time course analysis of hypoxia, granulation tissue and blood vessel growth, and remodeling in healing rat cutaneous incisional primary intention wounds. Wound Repair Regen 14:277–288.
Lopez-Barneo J, Gonzalez-Rodriguez P, Gao L, Fernandez-Aguera MC, Pardal R, Ortega-Saenz P. 2016a. Oxygen sensing by the carotid body: mechanisms and role in adaptation to hypoxia. Am J Physiol Cell Physiol 310:C629–C642.
Lopez-Barneo J, Macias D, Platero-Luengo A, Ortega-Saenz P, Pardal R. 2016b. Carotid body oxygen sensing and adaptation to hypoxia. Pflugers Arch 468:59–70.
Lotfy A, Salama M, Zahran F, Jones E, Badawy A, Sobh M. 2014. Characterization of mesenchymal stem cells derived from rat bone marrow and adipose tissue: a comparative study. Int J Stem Cells 7:135–142.
Lu T, Finkel T. 2008. Free radicals and senescence. Exp Cell Res 314:1918–1922.
Lu T, Parthasarathy S, Hao H, Luo M, Ahmed S, Zhu J, Luo S, Kuppusamy P, Sen CK, Verfaillie CM, Tian J, Liu Z. 2010. Reactive oxygen species mediate oxidized low-density lipoprotein-induced inhibition of oct-4 expression and endothelial differentiation of bone marrow stem cells. Antioxid Redox Signal 13:1845–1856.
Luczak MW, Roszak A, Pawlik P, Kedzia H, Kedzia W, Malkowska-Walczak B, Lianeri M, Jagodzinski PP. 2012. Transcriptional analysis of CXCR4, DNMT3A, DNMT3B and DNMT1 gene expression in primary advanced uterine cervical carcinoma. Int J Oncol 40: 860–866.
Ludin A, Gur-Cohen S, Golan K, Kaufmann KB, Itkin T, Medaglia C, Lu XJ, Ledergor G, Kollet O, Lapidot T. 2014. Reactive oxygen species regulate hematopoietic stem cell self-renewal, migration and development, as well as their bone marrow microenvironment. Antioxid Redox Signal 21:1605–1619.
Manley NR, Capecchi MR. 1998. Hox group 3 paralogs regulate the development and migration of the thymus, thyroid, and parathyroid glands. Dev Biol 195:1–15.
Mansouri A, Chowdhury K, Gruss P. 1998. Follicular cells of the thyroid gland require Pax8 gene function. Nat Genet 19:87–90.
Martin DS, Grocott MP. 2013. Oxygen therapy in critical illness: precise control of arterial oxygenation and permissive hypoxemia. Crit Care Med 41:423–432.
Mayo V, Sawatari Y, Huang CY, Garcia-Godoy F. 2014. Neural crest-derived dental stem cells--where we are and where we are going. J Dent 42:1043–1051.
Melchionna R, Romani M, Ambrosino V, D'Arcangelo D, Cencioni C, Porcelli D, Toietta G, Truffa S, Gaetano C, Mangoni A, Pozzoli O, Cappuzzello C, Capogrossi MC, Napolitano M. 2010. Role of HIF-1alpha in proton-mediated CXCR4 down-regulation in endothelial cells. Cardiovasc Res 86:293–301.
Michiels C. 2004. Physiological and pathological responses to hypoxia. Am J Pathol 164:1875–1882.

Mishina Y, Snider TN. 2014. Neural crest cell signaling pathways critical to cranial bone development and pathology. Exp Cell Res 325:138–147.
Mohyeldin A, Garzón-Muvdi T, Quiñones-Hinojosa A. 2010. Oxygen in stem cell biology: a critical component of the stem cell niche. Cell Stem Cell 7:150–161.
Moroz E, Carlin S, Dyomina K, Burke S, Thaler HT, Blasberg R, Serganova I. 2009. Real-time imaging of HIF-1alpha stabilization and degradation. PLoS One 4:e5077.
Morrison SJ, Csete M, Groves AK, Melega W, Wold B, Anderson DJ. 2000. Culture in reduced levels of oxygen promotes clonogenic sympathoadrenal differentiation by isolated neural crest stem cells. J Neurosci 20:7370–7376.
Morrison SJ, White PM, Zock C, Anderson DJ. 1999. Prospective identification, isolation by flow cytometry, and in vivo self-renewal of multipotent mammalian neural crest stem cells. Cell 96:737–749.
Morriss GM, New DA. 1979. Effect of oxygen concentration on morphogenesis of cranial neural folds and neural crest in cultured rat embryos. J Embryol Exp Morphol 54:17–35.
Mueller A, Schäfer BW, Ferrari S, Weibel M, Makek M, Höchli M, Heizmann CW. 2005. The calcium-binding protein S100A2 interacts with p53 and modulates its transcriptional activity. J Biol Chem 280:29186–29193.
Mundell NA, Labosky PA. 2011. Neural crest stem cell multipotency requires Foxd3 to maintain neural potential and repress mesenchymal fates. Development 138:641–652.
Nagoshi N, Shibata S, Kubota Y, Nakamura M, Nagai Y, Satoh E, Morikawa S, Okada Y, Mabuchi Y, Katoh H, Okada S, Fukuda K, Suda T, Matsuzaki Y, Toyama Y, Okano H. 2008. Ontogeny and multipotency of neural crest-derived stem cells in mouse bone marrow, dorsal root ganglia, and whisker pad. Cell Stem Cell 2: 392–403.
Nelms BL, Pfaltzgraff ER, Labosky PA. 2011. Functional interaction between Foxd3 and Pax3 in cardiac neural crest development. Genesis 49:10–23.
Nie Y, Han YC, Zou YR. 2008. CXCR4 is required for the quiescence of primitive hematopoietic cells. J Exp Med 205:777–783.
Noels H, Zhou B, Tilstam PV, Theelen W, Li X, Pawig L, Schmitz C, Akhtar S, Simsekyilmaz S, Shagdarsuren E, Schober A, Adams RH, Bernhagen J, Liehn EA, Doring Y, Weber C. 2014. Deficiency of endothelial CXCR4 reduces reendothelialization and enhances neointimal hyperplasia after vascular injury in atherosclerosis-prone mice. Arterioscler Thromb Vasc Biol 34:1209–1220.
Nombela-Arrieta C, Pivarnik G, Winkel B, Canty KJ, Harley B, Mahoney JE, Park SY, Lu J, Protopopov A, Silberstein LE. 2013. Quantitative imaging of haematopoietic stem and progenitor cell localization and hypoxic status in the bone marrow microenvironment. Nat Cell Biol 15:533–543.
O'Reilly MA. 2001. DNA damage and cell cycle checkpoints in hyperoxic lung injury: braking to facilitate repair. Am J Physiol Lung Cell Mol Physiol 281:L291–L305.
Paratore C, Goerich DE, Suter U, Wegner M, Sommer L. 2001. Survival and glial fate acquisition of neural crest cells are regulated by an interplay between the transcription factor Sox10 and extrinsic combinatorial signaling. Development 128:3949–3961.
Pardal R, Ortega-Saenz P, Duran R, Lopez-Barneo J. 2007. Glia-like stem cells sustain physiologic neurogenesis in the adult mammalian carotid body. Cell 131:364–377.
Park IH, Kim KH, Choi HK, Shim JS, Whang SY, Hahn SJ, Kwon OJ, Oh IH. 2013. Constitutive stabilization of hypoxia-inducible factor alpha selectively promotes the self-renewal of mesenchymal progenitors and maintains mesenchymal stromal cells in an undifferentiated state. Exp Mol Med 45:e44.
Pelekanos RA, Ting MJ, Sardesai VS, Ryan JM, Lim YC, Chan JK, Fisk NM. 2014. Intracellular trafficking and endocytosis of CXCR4 in fetal mesenchymal stem/stromal cells. BMC Cell Biol 15:15.
Platero-Luengo A, Gonzalez-Granero S, Duran R, Diaz-Castro B, Piruat JI, Garcia-Verdugo JM, Pardal R, Lopez-Barneo J. 2014. An O2-sensitive glomus cell-stem cell synapse induces carotid body growth in chronic hypoxia. Cell 156:291–303.
Raheja LF, Genetos DC, Wong A, Yellowley CE. 2011. Hypoxic regulation of mesenchymal stem cell migration: the role of RhoA and HIF-1alpha. Cell Biol Int 35:981–989.
Rezzoug F, Seelan RS, Bhattacherjee V, Greene RM, Pisano MM. 2011. Chemokine-mediated migration of mesencephalic neural crest cells. Cytokine 56:760–768.
Saini U, Gumina RJ, Wolfe B, Kuppusamy ML, Kuppusamy P, Boudoulas KD. 2013. Preconditioning mesenchymal stem cells with caspase inhibition and hyperoxia prior to hypoxia exposure increases cell proliferation. J Cell Biochem 114:2612–2623.
Santilli G, Lamorte G, Carlessi L, Ferrari D, Rota Nodari L, Binda E, Delia D, Vescovi AL, De Filippis L. 2010. Mild hypoxia enhances proliferation and multipotency of human neural stem cells. PLoS One 5:e8575.
Schioppa T, Uranchimeg B, Saccani A, Biswas SK, Doni A, Rapisarda A, Bernasconi S, Saccani S, Nebuloni M, Vago L, Mantovani A, Melillo G, Sica A. 2003. Regulation of the chemokine receptor CXCR4 by hypoxia. J Exp Med 198:1391–1402.
Schwarz D, Varum S, Zemke M, Scholer A, Baggiolini A, Draganova K, Koseki H, Schubeler D, Sommer L. 2014. Ezh2 is required for neural crest-derived cartilage and bone formation. Development 141:867–877.
Scully D, Keane E, Batt E, Karunakaran P, Higgins DF, Itasaki N. 2016. Hypoxia promotes production of neural crest cells in the embryonic head. Development 143:1742–1752.
Shen B, Zheng MQ, Lu JW, Jiang Q, Wang TH, Huang XE. 2013. CXCL12-CXCR4 promotes proliferation and invasion of pancreatic cancer cells. Asian Pac J Cancer Prev 14:5403–5408.
Shi D, Li X, Chen H, Che N, Zhou S, Lu Z, Shi S, Sun L. 2014. High level of reactive oxygen species impaired mesenchymal stem cell migration via overpolymerization of F-actin cytoskeleton in systemic lupus erythematosus. Pathol Biol (Paris) 62:382–390.
Shtukmaster S, Schier MC, Huber K, Krispin S, Kalcheim C, Unsicker K. 2013. Sympathetic neurons and chromaffin cells share a common progenitor in the neural crest in vivo. Neural Dev 8:12.
Shyamala K, Yanduri S, Girish HC, Murgod S. 2015. Neural crest: The fourth germ layer. J Oral Maxillofac Pathol 19:221–229.
Sieber-Blum M, Grim M. 2004. The adult hair follicle: cradle for pluripotent neural crest stem cells. Birth Defects Res C Embryo Today 72:162–172.
Sieber-Blum M, Grim M, Hu YF, Szeder V. 2004. Pluripotent neural crest stem cells in the adult hair follicle. Dev Dyn 231:258–269.
Sieber-Blum M, Hu Y. 2008. Epidermal neural crest stem cells (EPI-NCSC) and pluripotency. Stem Cell Rev 4:256–260.
Sigal AC, Keenan M, Lazova R. 2012. P75 nerve growth factor receptor as a useful marker to distinguish spindle cell melanoma from other spindle cell neoplasms of sun-damaged skin. Am J Dermatopathol 34:145–150.
Singleton Escofet R. 2013. Role of CXCR4 dynamics and activity in neural crest migration. In: Division of biosciences. London, UK: University College of London.
Speetjens FM, Liefers GJ, Korbee CJ, Mesker WE, van de Velde CJ, van Vlierberghe RL, Morreau H, Tollenaar RA, Kuppen PJ. 2009. Nuclear localization of CXCR4 determines prognosis for colorectal cancer patients. Cancer Microenviron 2:1–7.
Spinello I, Quaranta MT, Riccioni R, Riti V, Pasquini L, Boe A, Pelosi E, Vitale A, Foa R, Testa U, Labbaye C. 2011. MicroRNA-146a and AMD3100, two ways to control CXCR4 expression in acute myeloid leukemias. Blood Cancer J 1:e26.
Staller P, Sulitkova J, Lisztwan J, Moch H, Oakeley EJ, Krek W. 2003. Chemokine receptor CXCR4 downregulated by von Hippel-Lindau tumour suppressor pVHL. Nature 425:307–311.
Stevens A, Zuliani T, Olejnik C, LeRoy H, Obriot H, Kerr-Conte J, Formstecher P, Bailliez Y, Polakowska RR. 2008. Human dental pulp stem cells differentiate into neural crest-derived melanocytes and have label-retaining and sphere-forming abilities. Stem Cells Dev 17:1175–1184.
Suzuki A, Osanai T, Tanaka M, Tomita H, Magota K, Okumura K. 2014. Coupling factor 6 attenuates CXCR4 expression through the HIF-1alpha and c-Src pathways and promotes endothelial apoptosis and inflammation. Hypertens Res 37:708–715.
Takubo K, Goda N, Yamada W, Iriuchishima H, Ikeda E, Kubota Y, Shima H, Johnson RS, Hirao A, Suematsu M, Suda T. 2010. Regulation of the HIF-1alpha level is essential for hematopoietic stem cells. Cell Stem Cell 7:391–402.

Tan M, Heizmann CW, Guan K, Schafer BW, Sun Y. 1999. Transcriptional activation of the human S100A2 promoter by wild-type p53. FEBS Lett 445:265–268.
Thomas AJ, Erickson CA. 2009. FOXD3 regulates the lineage switch between neural crest-derived glial cells and pigment cells by repressing MITF through a non-canonical mechanism. Development 136:1849–1858.
Thorsen E, Haave H, Hofso D, Ulvik RJ. 2001. Exposure to hyperoxia in diving and hyperbaric medicine--effects on blood cell counts and serum ferritin. Undersea Hyperb Med 28:57–62.
Timofeev O, Schlereth K, Wanzel M, Braun A, Nieswandt B, Pagenstecher A, Rosenwald A, Elsasser HP, Stiewe T. 2013. p53 DNA binding cooperativity is essential for apoptosis and tumor suppression in vivo. Cell Rep 3:1512–1525.
Tomita Y, Matsumura K, Wakamatsu Y, Matsuzaki Y, Shibuya I, Kawaguchi H, Ieda M, Kanakubo S, Shimazaki T, Ogawa S, Osumi N, Okano H, Fukuda K. 2005. Cardiac neural crest cells contribute to the dormant multipotent stem cell in the mammalian heart. J Cell Biol 170:1135–1146.
Vieira HL, Alves PM, Vercelli A. 2011. Modulation of neuronal stem cell differentiation by hypoxia and reactive oxygen species. Prog Neurobiol 93:444–455.
Wahlbuhl M, Reiprich S, Vogl MR, Bosl MR, Wegner M. 2012. Transcription factor Sox10 orchestrates activity of a neural crest-specific enhancer in the vicinity of its gene. Nucleic Acids Res 40:88–101.
Wang J, Guan J, Lu Z, Jin J, Cai Y, Wang C, Wang F. 2015. Clinical and tumor significance of tropomyosin-1 expression levels in renal cell carcinoma. Oncol Rep 33:1326–1334.
Wang L, Wang Z, Yang B, Yang Q, Wang L, Sun Y. 2009. CXCR4 nuclear localization follows binding of its ligand SDF-1 and occurs in metastatic but not primary renal cell carcinoma. Oncol Rep 22:1333–1339.
Wang WD, Melville DB, Montero-Balaguer M, Hatzopoulos AK, Knapik EW. 2011. Tfap2a and Foxd3 regulate early steps in the development of the neural crest progenitor population. Dev Biol 360:173–185.
Wang Y, Yuan Z, You C, Han J, Li H, Zhang Z, Yan H. 2014. Overexpression p21WAF1/CIP1 in suppressing retinal pigment epithelial cells and progression of proliferative vitreoretinopathy via inhibition CDK2 and cyclin E. BMC Ophthalmol 14:144.
Wen X, Liu L, Deng M, Zhang L, Liu R, Xing Y, Zhou X, Nie X. 2012. Characterization of p75(+) ectomesenchymal stem cells from rat embryonic facial process tissue. Biochem Biophys Res Commun 427:5–10.
Wong CE, Paratore C, Dours-Zimmermann MT, Rochat A, Pietri T, Suter U, Zimmermann DR, Dufour S, Thiery JP, Meijer D, Beermann F, Barrandon Y, Sommer L. 2006. Neural crest-derived cells with stem cell features can be traced back to multiple lineages in the adult skin. J Cell Biol 175:1005–1015.
Xia T, Cheng H, Zhu Y. 2014. Knockdown of hypoxia-inducible factor-1 alpha reduces proliferation, induces apoptosis and attenuates the aggressive phenotype of retinoblastoma WERI-Rb-1 cells under hypoxic conditions. Ann Clin Lab Sci 44:134–144.
Yamaji R, Fujita K, Takahashi S, Yoneda H, Nagao K, Masuda W, Naito M, Tsuruo T, Miyatake K, Inui H, Nakano Y. 2003. Hypoxia up-regulates glyceraldehyde-3-phosphate dehydrogenase in mouse brain capillary endothelial cells: involvement of Na+/Ca2+exchanger. Biochim Biophys Acta 1593:269–276.
Yang X, Zhang W, van den Dolder J, Walboomers XF, Bian Z, Fan M, Jansen JA. 2007. Multilineage potential of STRO-1+rat dental pulp cells in vitro. J Tissue Eng Regen Med 1:128–135.
Yoshida S, Shimmura S, Nagoshi N, Fukuda K, Matsuzaki Y, Okano H, Tsubota K. 2006. Isolation of multipotent neural crest-derived stem cells from the adult mouse cornea. Stem Cells 24:2714–2722.
Zhang C, Qiang Q, Jiang Y, Hu L, Ding X, Lu Y, Hu G. 2015. Effects of hypoxia inducible factor-1alpha on apoptotic inhibition and glucocorticoid receptor downregulation by dexamethasone in AtT-20 cells. BMC Endocr Disord 15:24.
Zhang T, Woods TL, Elder JT. 2002. Differential responses of S100A2 to oxidative stress and increased intracellular calcium in normal, immortalized, and malignant human keratinocytes. J Invest Dermatol 119:1196–1201.
Zhong H, Simons JW. 1999. Direct comparison of GAPDH, beta-actin, cyclophilin, and 28S rRNA as internal standards for quantifying RNA levels under hypoxia. Biochem Biophys Res Commun 259:523–526.
Zhou D, Shao L, Spitz DR. 2014. Reactive oxygen species in normal and tumor stem cells. Adv Cancer Res 122:1–67.
Zhu W, Chen J, Cong X, Hu S, Chen X. 2006. Hypoxia and serum deprivation-induced apoptosis in mesenchymal stem cells. Stem Cells 24:416–425.